Global and Planetary Change 194 (2020) 103312

Contents lists available at ScienceDirect

Global and Planetary Change

journal homepage: www.elsevier.com/locate/gloplacha

Invited research article

Mercury linked to Deccan Traps volcanism, climate change and the end-Cretaceous mass extinction

Gerta Keller[a,*], Paula Mateo[b], Johannes Monkenbusch[c], Nicolas Thibault[c], Jahnavi Punekar[d], Jorge E. Spangenberg[e], Sigal Abramovich[f], Sarit Ashckenazi-Polivoda[g], Blair Schoene[a], Michael P. Eddy[h], Kyle M. Samperton[i], Syed F.R. Khadri[j], Thierry Adatte[k]

[a] Department of Geosciences, Princeton University, Princeton, NJ 08544, USA
[b] Division of Geological and Planetary Sciences, California Institute of Technology, Pasadena, CA 91125, USA
[c] Department of Geosciences and Natural Resource Management, University of Copenhagen, Copenhagen 1350, Denmark
[d] Department of Earth Sciences, Indian Institute of Technology Bombay, Mumbai 400 076, India
[e] Institute of Earth Surface Dynamics (IDYST), University of Lausanne, Lausanne 1015, Switzerland
[f] Department of Geological and Environmental Sciences, Ben Gurion University of the Negev, Beer Sheva, P.O.B. 653, 84105, Israel
[g] Dead Sea and Arava Science Center, Masada National Park, Mount Masada, Dead-Sea mobile post 86910, Israel
[h] Department of Earth, Atmospheric, and Planetary Sciences, Purdue University, West Lafayette, IN 47907, USA
[i] Nuclear and Chemical Sciences Division, Lawrence Livermore National Laboratory, Livermore, CA 94550, USA
[j] Department of Geology, Amravati University, Amravati, India
[k] Institute of Earth Sciences, University of Lausanne, Lausanne 1015, Switzerland

ARTICLE INFO

Keywords:
Deccan Traps volcanism
Mercury stratigraphy
End-Cretaceous
Mass extinction
Hyperthermal warming

ABSTRACT

Mercury (Hg) anomalies linked to Large Igneous Provinces (LIP) volcanism have been identified in sediments across all five major mass extinctions in Earth's history. This study tests whether Hg in marine sediments is a reliable proxy linking Deccan Traps volcanic eruptions to late Maastrichtian global climate warming and the mass extinction at the Cretaceous-Paleogene boundary (KPB). Our primary test site is the Elles section in Tunisia, the auxiliary Global Stratotype Section and Point (GSSP) to El Kef. Elles has the most complete marine sedimentary record and a high average sedimentation rate of ~4.7 cm/ky. We chose the Hor Hahar section in Israel to corroborate the geographic distribution of Hg fallout from Deccan volcanism. Reliability of the Hg proxy over the last 550 ky of the Maastrichtian to early Danian was evaluated based on high-resolution age control (orbital cyclostratigraphy), stable isotope climate record, Hg concentrations, biotic turnover and mass extinction. These results were correlated with the pulsed Deccan eruptive history constrained previously by U-Pb zircon geochronology.

Our results support Hg as robust proxy for Deccan volcanism with large Hg spikes marking “extreme event” (EE) pulsed eruptions correlative with climate warming peaks separated by steady, less intense eruptions. Long-term global climate warming began near ~350 ky pre-KPB, reached maximum warming (3–4 °C) between 285 and 200 ky pre-KPB, followed by gradual cooling and rapid temperature drop between 45 and 25 ky pre-KPB. During the last 25 ky before the KPB, multiple Hg EE eruptions correlate with hyperthermal warming that culminated in the rapid mass extinction at Elles during ≤1000 years of the Cretaceous. These latest Cretaceous Hg peaks may correlate with massive, distal, Deccan-sourced lava flows (> 1000 km long) that traversed the Indian subcontinent and flowed into the Bay of Bengal, bracketing the mass extinction. These results support Deccan volcanism as a primary driver of the end-Cretaceous mass extinction.

1. Introduction

The end-Cretaceous mass extinction at the Cretaceous-Paleogene boundary (KPB; 66.016 Ma) is perhaps the most easily explained environmental catastrophe due to a bolide impact on Yucatan and Deccan Traps volcanism in India. However, the relative importance of these events in driving extinctions is controversial. For the past 40 years, the impact theory has been favored as the almost unquestioned cause of the end-Cretaceous mass extinction, whereas volcanism of the Deccan Traps Large Igneous Province (LIP), today covering an area three times

* Corresponding author.
E-mail address: gkeller@princeton.edu (G. Keller).

https://doi.org/10.1016/j.gloplacha.2020.103312
Received 5 June 2020; Received in revised form 6 August 2020; Accepted 12 August 2020
Available online 03 September 2020
0921-8181/

that of France, was relegated to inconsequential secondary effects. Nonetheless, LIPs, defined as the largest volcanic eruptions in Earth's history (> 100,000 km^3; Ernst and Youbi, 2017), have long been interpreted as potentially linked to all major mass extinctions in Earth's history (Courtillot, 1999; Courtillot and Renne, 2003; Bond and Wignall, 2014; Bond and Grasby, 2017; Bond and Grasby, 2020). However, whether LIPs are the main cause of major biotic crises is still in dispute because extinctions in the fossil record are rarely observed directly within volcanic deposits. An exception is the Deccan Traps LIP where the end-Cretaceous mass extinction is bracketed between trans-India lava flows (> 1000 km long) (Keller et al., 2008, 2011, 2012; Self et al., 2008). These flows were sourced from the main Deccan volcanic province, where eruptions accumulated > 1,500,000 km^3 of basalt reaching a thickness of > 3400 m of which 3100 m (90%) accumulated over just ~750 ky spanning magnetochron C29r (Beane et al., 1986; Khadri et al., 1988; Chenet et al., 2008, 2009; Jay and Widdowson, 2008; Schoene et al., 2015; Kale et al., 2020).

Climate and environmental changes inferred from proxy records in sedimentary sequences spanning the end-Cretaceous mass extinction have been broadly linked to U-Pb ages of Deccan volcanism (Schoene et al., 2015, 2019) via biostratigraphy, magnetostratigraphy and orbital cyclostratigraphy (e.g., Keller, 2014; Punekar et al., 2014a; Thibault and Husson, 2016; Thibault et al., 2016; Barnet et al., 2018). Imprecise estimates of eruption timing, rates and incomplete sedimentary records have resulted in novel scenarios, including the Chicxulub impact as the trigger for a state shift in Deccan volcanism (Renne et al., 2015; Richards et al., 2015), or the end-Cretaceous mass extinction not related to major Deccan eruptions and associated climate change (Sprain et al., 2019; Hull et al., 2020; Chiarenza et al., 2020).

Linking Deccan Traps LIP volcanism to climate warming and the end-Cretaceous mass extinction requires a reliable proxy for volcanic emissions, as well as sedimentary sequences with complete bio- and chemo-stratigraphic records across the KPB. One such potential proxy is stratigraphic mercury (Hg). Volcanic eruptions are the main source of natural Hg to the atmosphere (Pyle and Mather, 2003; Pirrone et al., 2010). Following eruptions, Hg is distributed globally during its atmospheric residence time of six months to one year prior to precipitation and deposition in terrestrial and marine environments (Pyle and Mather, 2003; Fitzgerald et al., 2007; Percival et al., 2015; review in Grasby et al., 2019). Mercury anomalies in sediments of the Late Permian mass extinction yielded a promising LIP volcanism proxy (Sanei et al., 2012; Grasby et al., 2013), which marked a major turning point in mass extinction studies. Since then, all five major mass extinctions have yielded Hg anomalies in marine and terrestrial sediments, hypothesized to derive from LIPs, thus potentially providing a direct link between LIP volcanism, climate change and biotic crises (e.g., Grasby et al., 2016; Font et al., 2016; Thibodeau et al., 2016; Sial et al., 2016, 2020; Gong et al., 2017; Jones et al., 2017; Percival et al., 2017; Thibodeau and Bergquist, 2017; Shen et al., 2019; review in Grasby et al., 2019). However, testing the robustness of Hg as a volcanic proxy requires high-resolution Hg data from well-calibrated stratigraphic sections for comparison to detailed LIP eruption records.

In this study we test whether Hg is a reliable proxy for Deccan volcanic emissions in the time interval spanning from the late Maastrichtian through the KPB and end-Cretaceous mass extinction in the shallow marine sediments of Elles, Tunisia, the auxiliary Global Stratotype Section and Point (GSSP) to El Kef. Specifically, we evaluate whether Hg spikes reflect extreme event eruptions that can be correlated globally, whether these are linked to global climate warming, and whether the Deccan eruption history could have caused the end-Cretaceous mass extinction.

We assess the reliability of the Hg proxy for Deccan volcanism by developing a high-resolution database for the last 550 ky of the late Maastrichtian leading up to the KPB transition at the Elles section based on (a) biostratigraphy and orbital cyclostratigraphy as age control; (b) stable isotope climate record based on benthic foraminifera; (c) Hg deposition and potential concentration processes; (d) Hg stratigraphy; (e) global correlation of Hg extreme events between Tunisia and Israel; (f) correlation of Elles cyclostratigraphy and Hg records with Deccan Traps' U-Pb zircon geochronology and pulsed eruptions; and (g) global climate, Deccan volcanism and the end-Cretaceous mass extinction.

We thus evaluate Hg linked to Deccan volcanism, climate change and the end-Cretaceous mass extinction based on seven independent topics, each one yielding related evidence with the sum of their parts providing the strongest confirmation of volcanism-induced environmental changes. For clarification, we structure these topics (a-g) into separate sections (2–8), addressing the relevant key issues: (2) age control, (3) global climate change, (4) Hg potential concentration processes, (5) Hg stratigraphy, (6) global correlation of Hg extreme events, (7) Elles Hg correlated to Deccan volcanism, and (8) climate, volcanism and the mass extinction. Sections begin with a short introduction followed by methods, results and interpretation and discussion. Section 8 integrates the various topics with the mass extinction.

2. Elles age control: cyclostratigraphy

2.1. Introduction

The Elles section in Tunisia was chosen as the primary test site because of its complete, undisturbed and continuously exposed Maastrichtian through Danian sequence. Located 56 km southeast from the El Kef Global Stratotype Section and Point (GSSP) (Fig. 1), Elles is the auxiliary GSSP to El Kef where a major fault limits late Maastrichtian exposure to ~4 m below the KPB (Keller et al., 1995; Abramovich and Keller, 2002). During the late Maastrichtian to early Danian, Elles was located on the continental shelf of the Tethys seaway at 100–150 m paleodepth and received relatively high terrestrial runoff from North Africa (Fig. 1). Deposition consisted of marls, silty marls, shales and claystones (Abramovich and Keller, 2002; Stueben et al., 2003) at an average sedimentation rate of ~4.7 cm/ky. Samples were collected at 10-cm intervals for the Maastrichtian and at closer sample spacing (1, 2 and 3 cm) for the last 40 cm below the KPB and early Danian.

2.2. Methods

Our age model at Elles is based on cyclostratigraphy and planktic foraminiferal biostratigraphy (Fig. 2). Cyclostratigraphic analysis, based on the record of astronomically forced climate cycles in marine sedimentary sequences, yields age control with orbital cycles of precession (19–23 ky), obliquity (41 ky) and eccentricity (100 ky). For the astronomical calibration of the Elles section, cyclicity was determined based on percent calcite content (%$CaCO_3$) with the mean signal detrended by a lowess smoothing with a span of 35%. An Evolutive Fast Fourier transform of the detrended %$CaCO_3$ signal highlights significant periodicity for the 26 m below the KPB (Fig. A1). We interpret this periodicity as precession with a total of 27.5 cycles filtered from the %$CaCO_3$ signal (Fig. 2). Under the premise of a 20 ky period per precession cycle, we propose a duration of 550 ky for the 26 m below the KPB. The filtered precession cycles show a strong 100 ky modulation, which can also be filtered from the tuned signal (Fig. A2). This strong indication for the astronomic origin of the cyclicity is evidence for the completeness of the signal. More details on the cyclostratigraphy methodology as well as on planktic foraminiferal processing and analysis can be found in Appendix A (Section A.1).

2.3. Results

Planktic foraminiferal biostratigraphy zones CF3, CF2 and CF1 span the late Maastrichtian magnetochrons C30n and C29r below the KPB. Cyclostratigraphy at Elles now yields more precise durations for these

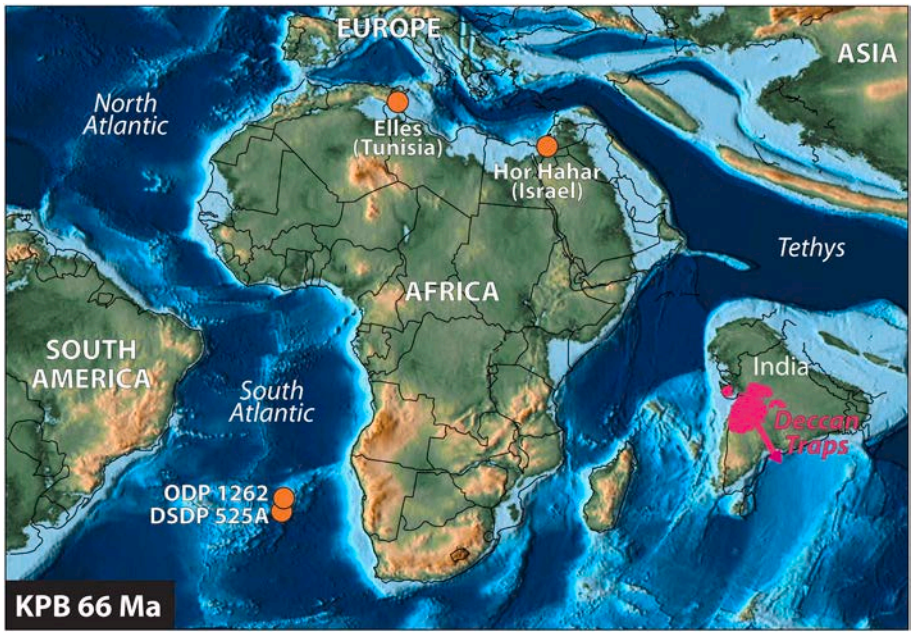

Fig. 1. Paleoceanographic map with KPB localities referred to in this study. Paleomap from Scotese (2013).

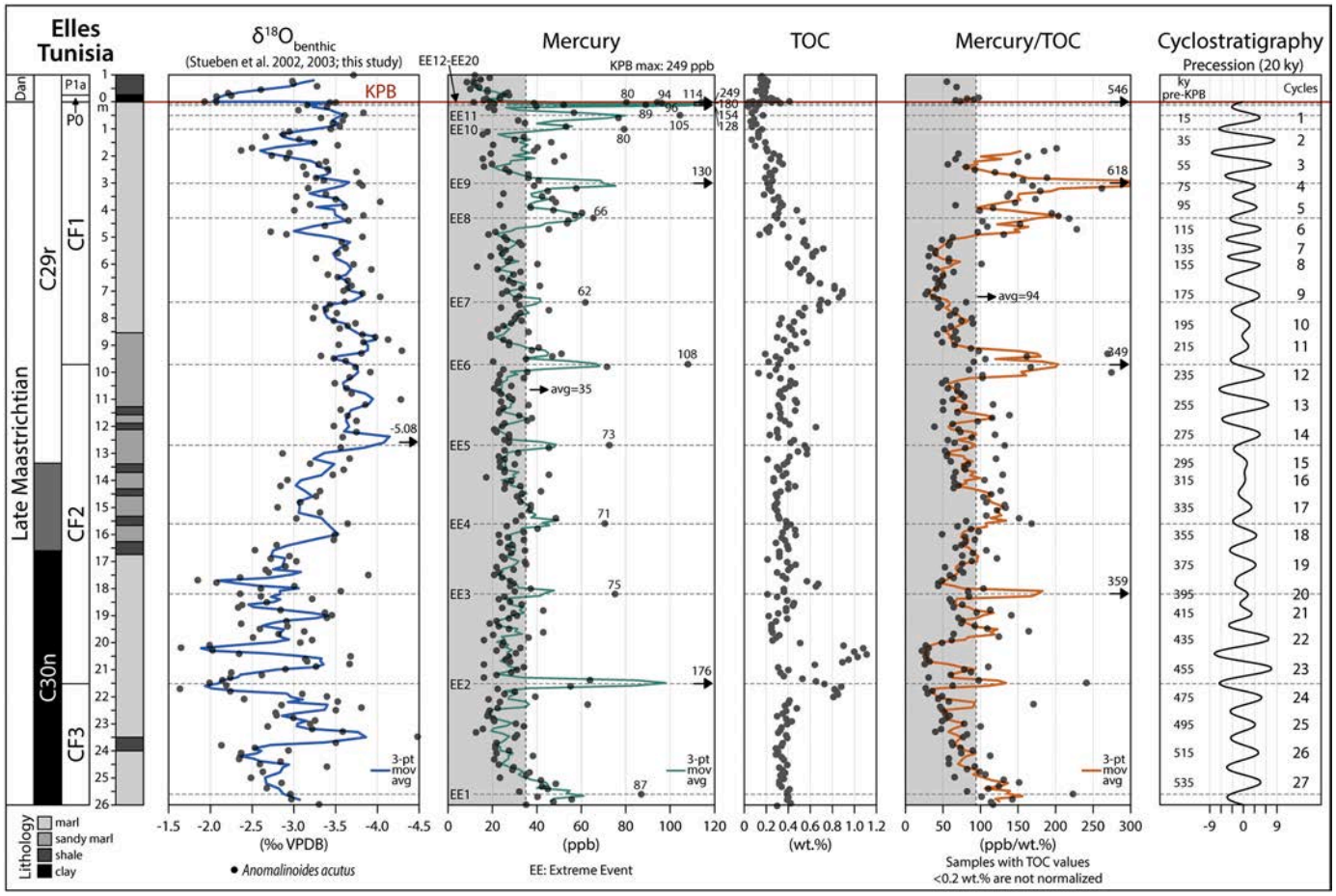

Fig. 2. High-resolution $\delta^{18}O$, Hg, TOC and Hg/TOC data at the astronomically tuned Elles section in Tunisia. Data are shown as 3-point average indicated by solid line. Note paroxysmal eruptions during the last 25 ky of the Maastrichtian ending with the end-Cretaceous mass extinction at the KPB. Hg/TOC data are normalized only for values > 0.2 wt%. $\delta^{18}O$ data from Stueben et al. (2002, 2003) and this study. ky: thousands of years.

zones (Fig. A3). The base of zone CF1 is defined by the first appearance (FA) of *Plummerita hantkeninoides* (9.6 m below the KPB) and spans 11.5 cycles or 229 ky ending at the KPB extinction horizon. Zone CF2 spans 240 ky from the last appearance (LA) of the *Gansserina gansseri* at the base (465 ky pre-KBP, 21.5 m, cycle 23.5) to the FA of *P. hantkeninoides* (Fig. 2). The base of zone CF3 has yet to be determined.

The magnetic reversal C30n/C29r serves as a global correlation point but magnetostratigraphy is absent at Elles. The duration of the pre-KPB portion of C29r has been estimated with both geochronological and cyclostratigraphic approaches. A U-Pb age for the KPB was calculated by Schoene et al. (2019), based on the U-Pb data of Clyde et al. (2016), to be 66.016 ± 0.050 Ma (95% confidence, internal errors only). Combined with an age of 66.296 + 0.037/−0.030 Ma for the C30n/C29r reversal within the Western Ghats of the Deccan Traps, Schoene et al. (2019) calculate a duration of 280 ± 60 ky for C29r below the KPB. This age agrees well with a more recent U-Pb age for the reversal from the Malwa Plateau of 66.266 + 0.060/−0.049 (Eddy et al., 2020).

2.4. Interpretation

Numerous cyclostratigraphic studies of marine sections from outcrops on land and from deep-sea cores yield estimates for the C30n/C29r duration to be between precession cycles 15 and 18.5 or about 335 ± 35 ky (Table A1) (review in Thibault and Husson, 2016). While the cyclostratigraphic estimates are on average marginally longer than U-Pb estimate, these two approaches overlap within uncertainty. Additionally, the C30n/C29r reversal has been observed in other sections within foraminiferal zone CF2, which overlaps with precession cycles 15–18.5 at Elles (Fig. 2). The agreement between these independent estimates gives confidence that the Deccan Traps eruption record can be correlated with the Hg data reported at Elles, albeit with uncertainties of tens of ky.

3. Global climate change linked to Deccan volcanism

3.1. Introduction

Global climate changes attributed to the Deccan Traps are not unique but rather common among LIP events, thought to have driven the five major mass extinctions in Earth's history (Courtillot, 1999; Courtillot and Renne, 2003; Bond and Wignall, 2014; Bond and Grasby, 2017; Bond and Grasby, 2020). Global climate warming during the late Maastrichtian magnetochron C29r has long been attributed to Deccan volcanism but direct causal evidence was largely lacking (e.g., McLean, 1985; Li and Keller 1998a; Courtillot, 1999; Stueben et al., 2003; Punekar et al., 2014a; Thibault and Husson, 2016; Barnet et al., 2018). Climate warming is interpreted as the result of atmospheric accumulation of carbon dioxide (CO_2) followed by other highly heat-trapping greenhouse gases (e.g., sulfur-bearing gases, methane, light hydrocarbons) emitted by volcanic eruptions (Allard et al., 1994; Robock, 2000; Aiuppa et al., 2005; Chenet et al., 2007, 2008, 2009). These gases perturb the carbon cycle and lead to long-term climate warming over several hundred thousand years due to slow CO_2 removal from the atmosphere, mainly by drawdown into oceans and chemical weathering of fresh basalt (~10 to ~100 ky; Dessert et al., 2003; Chenet et al., 2007, 2008, 2009; Taylor et al., 2012). Other carbon-based greenhouse gases in volcanic emissions include thermogenic or abiotic methane and two- to four-carbon hydrocarbons (e.g., Taran and Giggenbach, 2003; Etiope et al., 2007; Fiebig et al., 2007; Etiope and Sherwood Lollar, 2013). These light hydrocarbons may have also contributed considerably to the greenhouse periods associated to LIPs. Volcanogenic sulfur dioxide (SO_2) and hydrogen sulfide (H_2S) combine with water vapor in the atmosphere to form sulfuric acid (H_2SO_4) and rain out as acid rain within weeks. When these gases are spewed into the stratosphere, they reside > 1 yr and reflect solar radiation back, resulting in short-term cooling (e.g., Giggenbach, 1980; Robock, 2000). A semi-quantitative discussion on CO_2 versus SO_2 volumes, fluxes and climatic consequences of Deccan volcanism is given in Chenet et al. (2008, 2009).

3.2. Methods

For the Elles Late Maastrichtian climate record during C29r, oxygen and carbon isotopes of the benthic and planktic foraminifera (*Anomalinoides acutus* and *Rugoglobigerina rugosa*, respectively) were first analyzed at 20 cm intervals (Stueben et al., 2002, 2003). In this study we doubled the sample resolution to 10 cm intervals and extended the sequence through the entire magnetochron C29r and upper C30n. Across the KPB transition, we increased sample resolution to 1 cm and 3 cm intervals (Fig. A6). The new analyses from additional intervals were performed at the Institute of Earth Surface Dynamics, University of Lausanne, Switzerland, using a Thermo Fisher Scientific (Bremen, Germany) carbonate-preparation device and Gas Bench II connected to a Thermo Fisher Delta Plus XL isotope ratio mass spectrometer. The stable carbon and oxygen isotope ratios were reported in the delta (δ) notation as the per mil (‰) relative to the Vienna Pee Dee belemnite standard (VPDB). The analytical uncertainty (1σ) estimated from replicate analyses of the international calcite standard NBS-19 and the laboratory standard Carrara Marble was better than ± 0.05‰ for $\delta^{13}C$ and ± 0.1‰ for $\delta^{18}O$.

Potential diagenetic alteration was evaluated based on the relationship between $\delta^{18}O$ and $\delta^{13}C$ (after Stueben et al., 2003). The narrow $\delta^{18}O$ range and lack of statistically significant correlation between $\delta^{18}O$ and $\delta^{13}C$ values of benthic foraminifera shells (Fig. A4) indicate minor diagenetic modification of their primary isotopic composition. Thus, $\delta^{18}O$ of benthic foraminifera at Elles can be confidently used as chemostratigraphic proxy for temperature variations of bottom water at 100–150 m depth. Planktic foraminifera are compromised by diagenesis and not used for isotopic interpretation in this study. More details on the assessment of diagenesis can be found in Appendix A (Section A.2).

3.3. Results

The $\delta^{18}O$ values were plotted as dots with a line representing the 3-point moving average (Fig. 2). In the lower part of the Elles section (26 m to 17 m, 545–375 ky pre-KPB), $\delta^{18}O$ values fluctuated rapidly (~1.5‰). Between 17 m and 12.5 m, $\delta^{18}O$ values decreased by 1.5‰ followed by relatively steady minima (−3.5‰ to −4.0‰) from 12.5 m to 8.5 m across the zone CF2/CF1 transition. Slightly increasing fluctuating values between 8.5 m and 2.5 m rapidly dropped from average −2.75‰ to −3.5‰ at 1.8 m. The last 1 m below the KPB marks the sudden return to −3.6‰ $\delta^{18}O$ values, except for a short increase by −0.5‰, ending with −3.5‰ at the KPB (Fig. 2).

3.4. Interpretation and discussion

The upper C30n at Elles between 545 and 375 ky pre-KPB marks a climate transition from the cooler Late Maastrichtian to prolonged climate warming, though the reason for these unusually high fluctuations is uncertain (Fig. 2). The persistent warming trend began near the base of C29r (cycle 18, 355 ky pre-KPB) and reached maximum temperatures by 280 ky (increase of 3.2 to 4 °C). In deep-sea sections the onset of Deccan-related climate warming is generally placed at ~300 ky pre-KPB. High temperatures persisted across the CF2/CF1 boundary (229 ky), then gradually decreased until 70 ky (cycle 3.5), followed by rapid 3–4 °C cooling by 45 ky (cycle 2.5) persisting until 25 ky (cycle 1.5) (Fig. 2). This short global cool event ended 1 m, or ~25 ky, below the KPB when climate warmed suddenly by ~2.5 °C resulting in

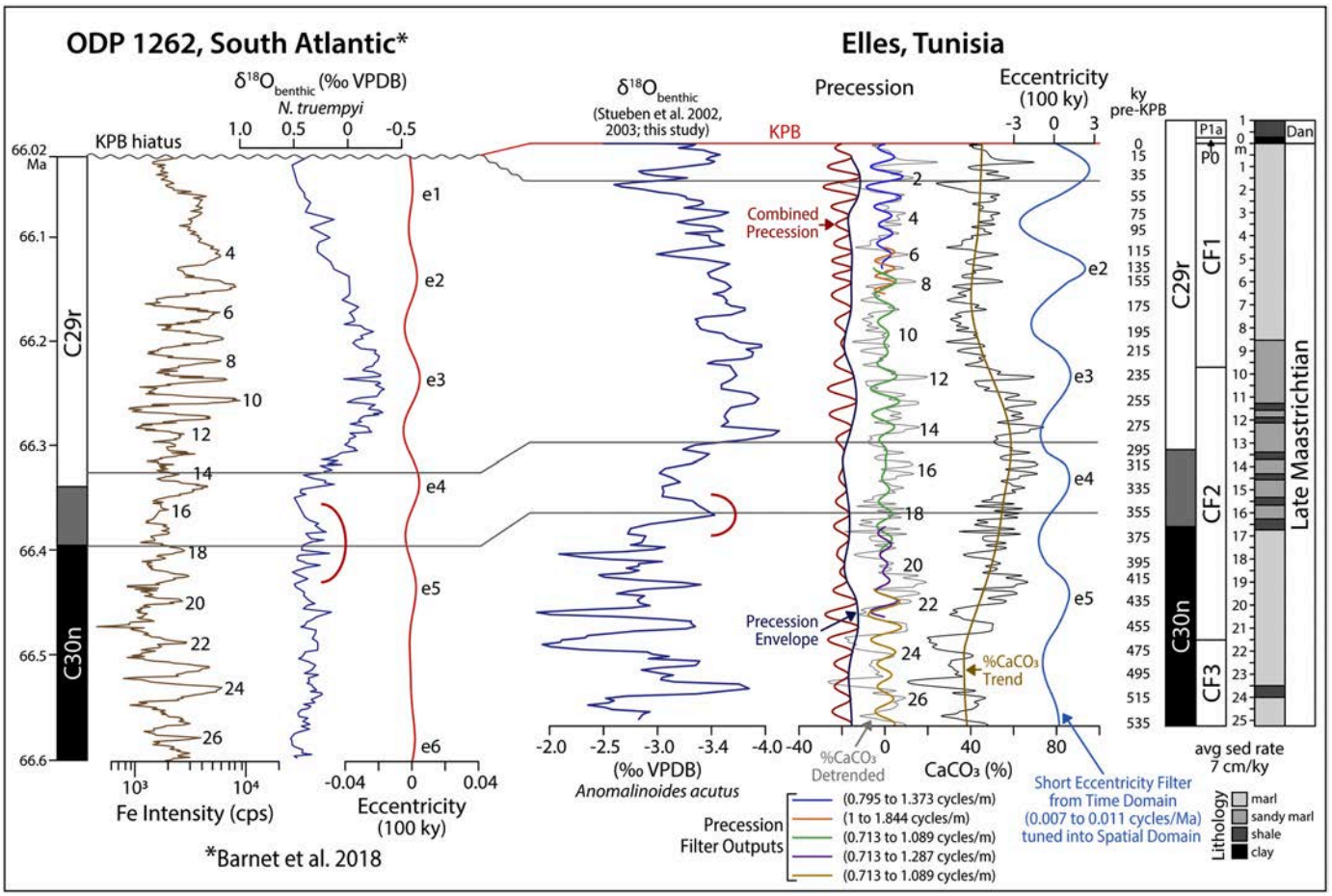

Fig. 3. Correlation of South Atlantic deep-sea ODP Site 1262 and Elles, Tunisia, based on $\delta^{18}O$ and orbital cyclostratigraphy. Note the KPB hiatus at Site 1262 indicates at least the last 40 ky below the KPB are missing including the hyperthermal warming present at Elles.

hyperthermal warming that culminated in the mass extinction (Fig. 2). In the earliest Danian, temperatures suddenly dropped to the coldest climatic conditions since C30n.

The C29r long-term climate warming is well known from deep-sea and terrestrial sequences and generally ends in the short-term cooling (cycles 2.5 to 1.5) between 45 ky to 25 ky pre-KPB. In deep-sea sections, part or all of this cooling generally underlies the KPB due to common erosion/hiatus patterns across the KPB (e.g., Sites 516, 528, 525A, 1209, 1262, 1267, Bidart, Gamsbach, Bottaccione; Keller, 1993; Li and Keller 1998a; Westerhold et al., 2008; Punekar et al., 2016; this study). The hyperthermal warming of the last 25 ky of the Maastrichtian, ending in the mass extinction, is thus missing in the deep-sea due to this erosion/hiatus pattern. Nevertheless, the assumption that deep-sea sites have continuous sedimentation across the KPB has led some scientists to conclude the cooling underlying the KPB indicates that CO_2 outgassing related to Deccan volcanism ended well prior to the end-Cretaceous mass extinction at the KPB, and therefore the Chicxulub impact is the sole cause for this biotic crisis (e.g., Henehan et al., 2016; Barnet et al., 2018; Hull et al., 2020; Chiarenza et al., 2020). A comparison between Elles and South Atlantic Site 525A (Li and Keller 1998a) revealed a hiatus across the KPB into the underlying cool event (Punekar et al., 2014a). The same pattern is observed for South Atlantic Site 1262 (Barnet et al., 2018). Compared with Elles, the KPB hiatus in these deep-sea sites spans precession cycles 1 and 2 (~35–40 ky). Further discussion on Sites 525A and 1262 age models can be found in Appendix A (Section A.5).

The complete and expanded sedimentary record at Elles demonstrates this short global cool event ended 1 m, or 25 ky, below the KPB when climate warmed rapidly by ~2.5 °C resulting in hyperthermal warming that culminated in the mass extinction (Fig. 2). Finally, in the earliest Danian (zone P0) temperatures suddenly dropped to the coldest climatic conditions since C30n.

4. Mercury: a proxy for Deccan volcanism

4.1. Introduction

Volcanism is the most important natural source of Hg to the atmosphere, with a residence time of six months to a year during which Hg is globally distributed prior to precipitation and deposition in terrestrial and marine environments (review in Grasby et al., 2019). In marine environments, direct atmospheric fallout of Hg accounts for about 70% while the other 30% is bound to organic matter (OM) and transported by rivers into ocean margins, of which only 28% reaches the open ocean (Amos et al., 2014; Holmes et al., 2010). In marginal marine sediments, Hg is primarily adsorbed onto OM yielding Hg spikes during pulsed LIP eruptions (Amos et al., 2014; Fitzgerald and Lamborg, 2014; review in Grasby et al., 2019). Model results for LIP eruptions during the end-Permian mass extinction predict that Hg emissions orders of magnitudes greater than normal background conditions could have generated a series of toxic shocks, each lasting > 1000 years (Grasby et al., 2020). Similar conditions likely prevailed during the maximum Deccan eruption pulse and hyperthermal warming near the end-Cretaceous mass extinction.

4.2. Atmospheric mercury fallout vs adsorption onto sediments

Long-term Hg sequestration in marine sediments occurs mostly through adsorption of Hg onto organic matter (OM) (e.g., Cranston and Buckley, 1972; Andren and Harriss, 1975; Outridge et al., 2007; Gehrke et al., 2009; Charbonnier et al., 2020), but it could also be driven by adsorption of Hg onto clay minerals (Krupp, 1988; Kongchum et al., 2011), Hg bound to iron-oxides in oxic environments (e.g., Kim et al., 2004; Mangold et al., 2014), formation of Hg-sulphides (Bower et al., 2008; Han et al., 2014) or adsorption of Hg onto pyrite in anoxic environments (Sanei et al., 2012; Yang et al., 2018; Shen et al., 2019; Them II et al., 2019; Grasby et al., 2019). Changes in Hg concentrations in marine sedimentary records could thus be associated not only to changes in the atmospheric Hg reservoir (e.g., volcanism) but also to changes in the marine environmental conditions (e.g., primary productivity, oxygenation, terrestrial input). Hence, in order to confidently interpret the Hg anomalies in marine sediments as the result of increased volcanic activity, it is critical to address other potential sources of change in Hg concentration.

4.2.1. Mercury and organic matter

Most of volcanic-sourced Hg is emitted as gaseous Hg^0 which is then oxidized to water-soluble Hg^{2+}, allowing direct deposition from the atmosphere onto both land and oceans through precipitation (e.g., Schroeder and Munthe, 1998; Grasby et al., 2019). In aquatic systems, Hg has a strong affinity for organic matter reflected by increased Hg concentration in organic-rich deposits compared to other sediments (Sanei et al., 2012). In near-shore environments, one of the most important Hg sources are terrestrial environments which deliver Hg bound to OM through riverine runoff, as first demonstrated by Grasby et al. (2017).

Changes in OM deposition (input of terrestrial OM, marine production/consumption of OM) therefore play a major role in Hg accumulation in marine sediments (Outridge et al., 2007; Gehrke et al., 2009; Stern et al., 2009), demonstrated by a strong correlation between Hg and organic carbon in numerous sedimentary sequences (Outridge et al., 2007; Gehrke et al., 2009; Grasby et al., 2013, 2019; Charbonnier et al., 2020). Hence, Hg concentrations are normalized against total organic carbon (TOC) contents in order to ensure that Hg enrichments are not directly related to increased OM accumulation and/or preservation (e.g., Sanei et al., 2012; Grasby et al., 2013; Sial et al., 2016; Percival et al., 2015). To avoid potential errors related to near-detection-limit TOC values and artificially magnified Hg/TOC anomalies, it has been proposed that Hg/TOC values should not be calculated for samples with < 0.2 wt% TOC (Grasby et al., 2013, 2019).

At the Elles section, Hg concentrations exhibit a weak correlation with TOC contents in the case where all TOC values are included ($r = -0.12$, $n = 291$) as well as in the case where only > 0.2 wt% values are used ($r = 0.02$, $n = 243$) (Fig. 4, Fig. A7). The highest Hg concentrations correspond to the lowest TOC contents, especially in the latest Maastrichtian (Fig. A8). Moreover, a strong correlation is observed between Hg and Hg/TOC also in the cases where all TOC values are included ($r = 0.72$, n = 291) and where only > 0.2 wt% values are used ($r = 0.81$, n = 243) (Fig. 4, Fig. A7). These results indicate that Hg enrichment in this data set is not controlled by changes in OM deposition.

4.2.2. Mercury and clay minerals

While in open marine environments Hg deposition is mostly atmospheric through precipitation, Hg deposition in near-shore environments is mostly sourced through riverine runoff (Grasby et al., 2017; Percival et al., 2018; Them II et al., 2019). As Hg sequestration in marine sediments is partly driven by adsorption of Hg onto clay minerals (Farrah and Pickering, 1978; Krupp, 1988; Kongchum et al., 2011), an increase in terrestrial input into the oceans primarily due to increased erosion on land and/or sea level drop could potentially lead to increased Hg concentrations in the sedimentary record.

At Elles, the relation between clay minerals and Hg is evaluated by normalizing Hg concentrations against phyllosilicate content. Hg concentrations are weakly correlated with phyllosilicates ($r = -0.02$, $n = 278$; Fig. 4, Fig. A7) even when focusing on only the top 2 m across the KPB, where the correlation is weakly moderate but inverse ($r = -0.41$, $n = 37$; Fig. 4, Fig. A8). In addition, Hg concentrations show a high degree correlation with Hg/phyllosilicates values ($r = 0.89$, n = 278) (Fig. 4, Fig. A7) thus confirming that changes in terrestrial input play no major role in Hg enrichments.

4.2.3. Mercury, pyrite and iron-oxides

Several studies have shown that Hg could be hosted primarily by sulfides in reducing conditions by the formation of Hg-sulfides or adsorption onto pyrite, leading to Hg enrichments in sulfide-rich sediments due to local Hg cycling (e.g., Wolfenden et al., 2005; Bower et al., 2008; Bouffard and Amyot, 2009; Sanei et al., 2012; Yang et al., 2018; Grasby et al., 2019; Shen et al., 2019; Them II et al., 2019). More specifically, Sanei et al. (2012) originally proposed that Hg/TOC spikes are driven by increased Hg-sulfide drawdown when there is excess volcanic derived Hg. In this case, the normal OM drawdown process is overwhelmed by excess Hg loading from the LIP eruption, and it is the additional sulfide drawdown that creates the Hg/TOC spikes. More details are discussed in Grasby et al. (2019) who also argue that this drawdown process drives the Hg/TOC spikes.

At Elles, fresh pyrite was not observed but iron-hydroxides (mainly goethite) were commonly observed at the KPB, where Hg enrichments are the highest, and in the Danian. Given that this mineral is of late diagenetic origin and mainly results from iron-sulfides oxidation in arid and semi-arid areas such as Elles, a transfer of Hg from pyrite to goethite is evident. The correlation between Hg and goethite is small when focusing on the top 2 m across the KPB ($r = 0.15$, $n = 28$; Fig. 4, Fig. A8), but high when considering only the KPB and Danian ($r = 0.69$, $n = 18$; Fig. 4, Fig. A8), implying that part of the Hg enrichments maybe linked to the presence of (now oxidized) iron sulfides, particularly at the KPB clay layer when goethite content reaches maximum (14.1%). Significant amounts of gypsum are also present at and right above the KPB. This Ca-sulfate was most probably formed by oxidation of pyrite and consequently account for part of the Hg enrichments. The correlation between Hg and gypsum is low (r = 0.02, $n = 11$; Fig. 4, Fig. A8), but may still imply some dependence of Hg on gypsum, particularly at the KPB.

Potential reducing conditions across the KPB are assessed by studying the concentration distribution of vanadium (V), which represents one of the most strongly enriched elements in anoxic, organic-rich sediments (e.g., Holland, 1984; Brumsack, 1986; Morford and Emerson, 1999; Tribovillard et al., 2006). At Elles, vanadium normalized against aluminium (V/Al) shows only a slight enrichment at the KPB, coincident with the organic-rich clay layer, therefore implying deposition in dysoxic to anoxic conditions (Fig. A8). The correlation between Hg and V/Al for the KPB and Danian samples is high ($r = 0.90$, $n = 17$; Fig. 4, Fig. A8) indicating that Hg enrichments are mostly related to changing redox conditions, particularly at the KPB (i.e., an eruption that increases Hg as well as drives anoxia). In contrast, the correlation between these variables in the latest Maastrichtian is low ($r = -0.15$, $n = 13$; Fig. 4, Fig. A8) thus suggesting that the observed Hg anomalies below the KPB are not driven by changes in local redox conditions.

4.2.4. Mercury and climate change (Milankovitch forcing)

In order to further test whether Hg content in the Elles section could originate from sources other than Deccan volcanism, we tested this signal for a possible imprint of sediment composition, climate change, and hence Milankovitch forcing, through its potential relationships to $CaCO_3$ and TOC contents. There is no significant correlation between $CaCO_3$ and Hg (Fig. A9a). There is a very weak negative correlation

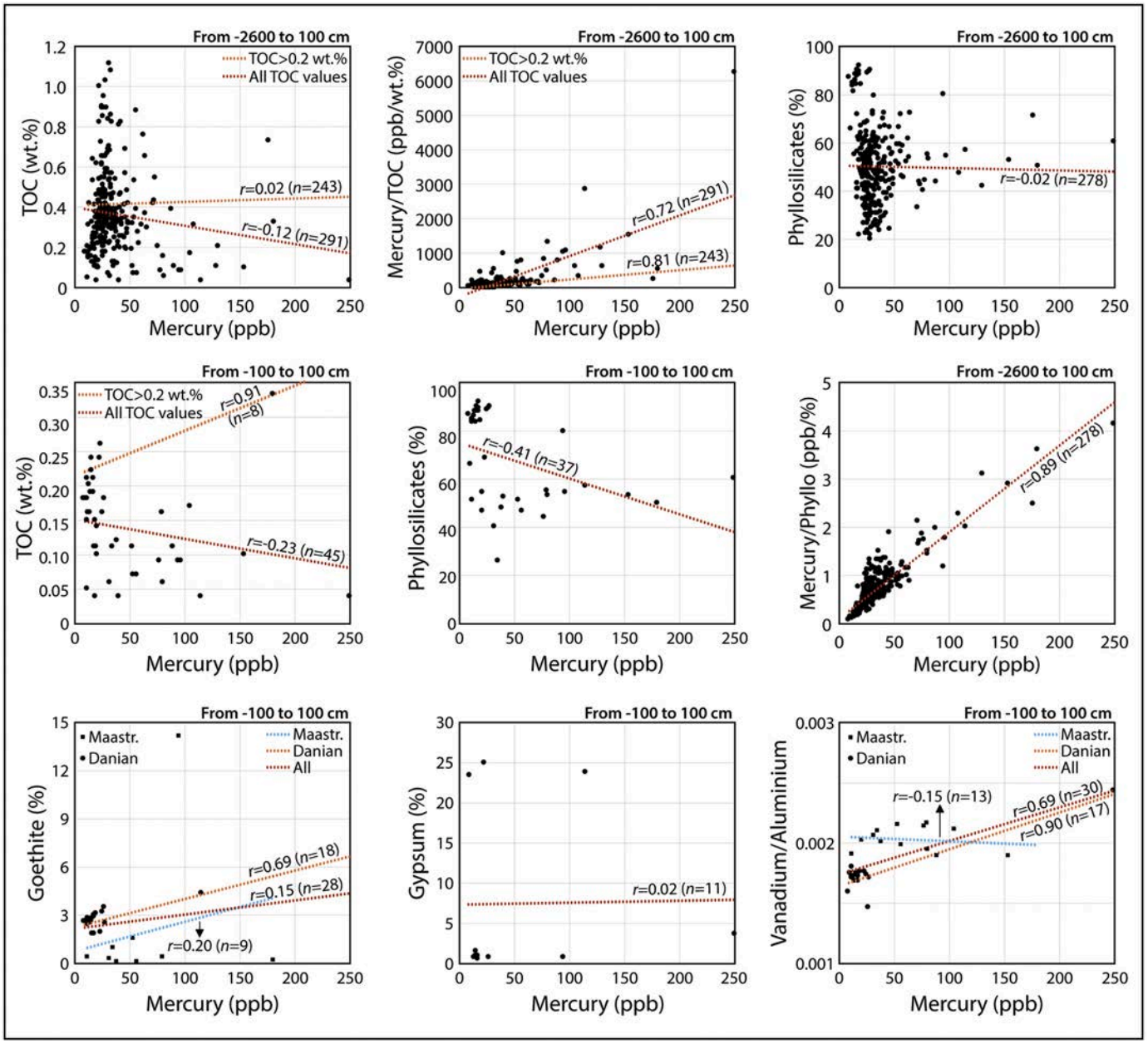

Fig. 4. Cross-plots of TOC and mercury, mercury/TOC and mercury, phillosilicates and mercury, mercury/phyllosilicates and mercury, goethite and mercury, gypsum and mercury, and Vanadium/Aluminium and mercury in the late Maastrichtian and across the Cretaceous-Paleogene boundary at the Elles section in Tunisia. Mineralogy data from Stueben et al. (2002, 2003), major and trace element data from B. Gertsch.

between $CaCO_3$ and TOC and the two intervals of enrichment in TOC are within more clayey lithologies (Fig. A9b, c). However, no covariance is observed between TOC and Hg (Fig. A9c); Hg spikes are clearly independent from TOC levels, showing enrichments in sediments with both low and high TOC content. The results of a 2π-multi-taper method (MTM) periodogram for Hg performed in the time domain are negative (Fig. A9d). There is no significant frequency in Hg within the precession band. Most of the eccentricity band also appears non-significant apart from a poorly significant peak at 97 ky (just above the 90% confidence level) situated at the right edge of this band. This peak belongs to a family of more significant peaks that extends to frequencies up to 0.148 cycles/ky (67 ky) and hence shows no clear relation to Milankovitch forcing (Fig. A9d).

We also tested a MTM cross-spectral coherency and phase between Hg and $CaCO_3$ contents in the time domain using the age calibration derived from our cyclostratigraphic analysis. The MTM cross-spectral analysis was performed using the script developed for MATLAB® by Huybers and Denton (2008). We chose to focus further on the relationship to $CaCO_3$ as this is the proxy used in our study to derive our cyclostratigraphic time scale. A strong Milankovitch imprint could be demonstrated by the strong precession and slight expression of the 100 ky eccentricity. The results of the cross-spectral analysis are also negative. No significant peaks can be delineated above the 95% confidence level in the two Milankovitch bands of the precession and short-eccentricity, suggesting that it is unlikely to have a common Milankovitch influence in both the Hg and $CaCO_3$ signals (Fig. A9e).

4.2.5. Summary of Hg enrichments

Hg enrichments at Elles appear to be unrelated to Milankovitch forcing, organic matter accumulation, riverine runoff or reducing conditions, except at the KPB clay layer where increased TOC content and V/Al suggest dysoxic-anoxic conditions that could have led in part to

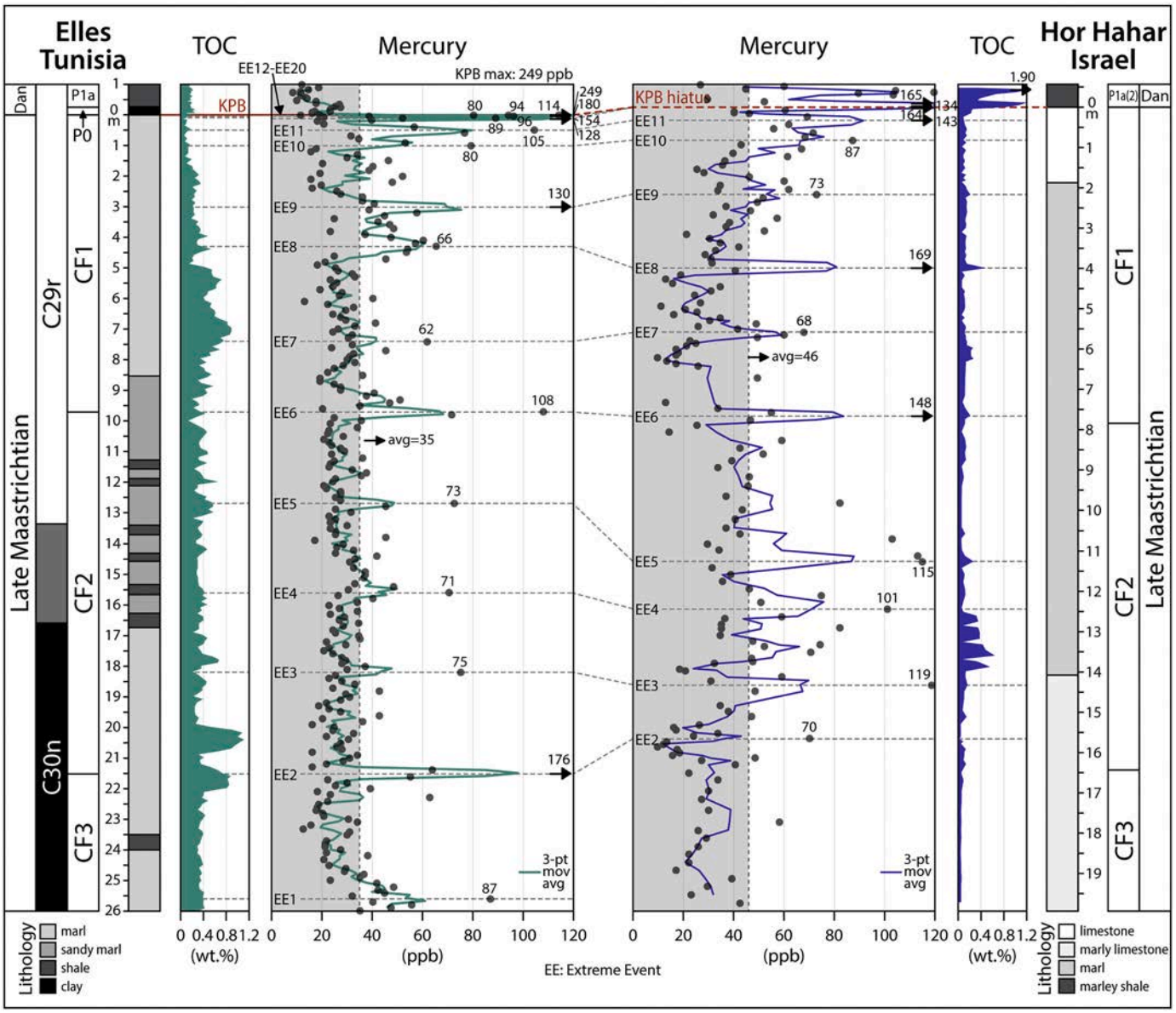

Fig. 5. Comparison of mercury (Hg) loading at Elles, Tunisia, with Hor Hahar, Israel, to evaluate the global distribution of Hg from Deccan eruptions. Note that most extreme events (EE) are present at Hor Hahar, including the onset of hyperthermal warming although there is a significant hiatus ranging from the early Danian across the KPB to EE12. Hg loading is on average higher at Hor Hahar (46 ppb) than at Elles (35 ppb), which may be a function of proximity to India. Note the 3-point average of Hg loading (solid line) underestimates extreme events, which are mostly Hg measurements in single samples of mm thin layers representing Hg concentrations. For this reason, the real Hg ppb values are added to the data points above the 3-point average line. Hg/TOC normalization was avoided because most samples in the Hor Hahar section measure TOC < 0.2 wt%.

enhanced Hg scavenging from the water column and deposition into sediments by pyrite adsorption (i.e., iron-hydroxides, gypsum). This assessment, along with the presence of Hg spikes across the KPB in other locations , is consistent with the hypothesis that the Hg record at Elles, and in particular the anomalies in the Maastrichtian including maxima immediately below the KPB, is the result of enhanced volcanic activity that can be traced to the eruption of the Deccan Traps in India.

5. Mercury stratigraphy at Elles, Tunisia

5.1. Introduction

We tested atmospheric fallout and terrestrial input of Hg into the shallow, middle continental shelf (~100–150 m depth) environment of Elles, Tunisia, over the last 550 ky of the Maastrichtian and across the KPB and end-Cretaceous mass extinction into the early Danian. The long record analyzed at high sample resolution (10 cm, 3 cm, 1 cm) was expected to reveal the ebb and flow of the Deccan eruption pulses. The coeval sample analysis of oxygen isotopes was expected to reveal the effects of CO_2 and SO_2 emissions from Deccan Traps on climate and environmental conditions.

5.2. Methods

Bulk-rock Hg was analyzed at Princeton University using the Zeeman R-915F (Lumex, St. Petersburg, Russia) high frequency atomic absorption spectrometer specifically designed for Hg determination with a detection limit of 0.3–3.0 ppb. Measurements are based on the direct thermal evaporation of Hg from solid samples. Analyses were done in duplicates and further repeated for very high Hg concentrations. Accuracy was assessed based on certified reference materials (1642a NIST standard, Hg calibrated at 30.2 ppb). Precision based on

relative standard deviation of repeated sample measurements was 5–10%. Excellent correspondence to the certified value was obtained with a correlation coefficient of 0.99 and a standard residual deviation of 0.44.

Total organic carbon (TOC) contents were determined at the University of Lausanne, Switzerland based on RockEval™ 6 and quantified by flame-ionization and infrared detection. The IFP 160000 RockEval standard was used for calibration. Analytical precision is 0.05 wt %.

5.3. Results

Hg concentrations at Elles revealed a distinct pattern of relatively constant values between 20 and 35 ppb and Hg spikes between 70 and 180 ppb, with the maximum of 249 at the KPB. TOC varied between 0.2 and 0.45 wt%, except during the last 35 ky pre-KPB when TOC was very low (< 0.2 wt%) (Fig. 2). Hg/TOC varied between 25 and 75 ppb/wt% and Hg spikes between 160 to > 600 ppb/wt% yielding an average of 93 ppb/wt%. We define Hg and Hg/TOC spikes above average concentrations (Hg > 35 ppb, Hg/TOC > 94 ppb/wt%) as "extreme events" (EE). The plots smoothed by 3-point moving average significantly lowered EE spikes, which are often single analyses of mm-size sediment layers, interpreted as Hg fallout. We interpret these Hg EE spikes serve well as first approximations of extreme volcanic events (Fig. 2). In this study we prefer to use direct Hg data as a proxy for Deccan volcanism instead of Hg/TOC data. Although we show for Elles that TOC played no major role in concentrating Hg above average levels, we present the Hg/TOC data for comparison.

5.4. Interpretation and discussion

A total of 20 extreme events (EE1 to EE20) can be identified during the last 550 ky of the late Maastrichtian at Elles and all but EE2 correlate with warming (Fig. 2). Interestingly, this correlation matches modeling results of Grasby et al. (2020) that predict a series of Hg spikes related to a fractal eruption pattern of a LIP event. At Elles, the oldest extreme events, EE1 to EE3, are in magnetochron C30n with ages 543 ky, 465 ky and 395 ky pre-KPB (Fig. 2). EE2 coincided with the extinction of *Gansserina gansseri* that marks the zone CF3/CF2 boundary (465 ky pre-KPB) at a time of cooling, sea level fall and high TOC (0.9 wt%), which is repeated at 445 ky pre-KPB suggesting erosion and increased terrestrial OM input correlative with a hiatus in many other localities (Keller et al., 2016; Mateo et al., 2017). These three extreme events predate the globally recognized warming attributed to Deccan volcanism in C29r, consistent with geochronology from the Malwa plateau, India, showing Deccan eruptions began ~100 ky or more prior to C29r (Schöbel et al., 2014; Eddy et al., 2020). Alternatively, these events may be a manifestation of recurrent earlier eruptions (Keller, 2003; Mateo et al., 2017; Sheth et al., 2017; Verma and Khosla, 2019).

Chron C29r marks long-term climate warming from the base at 355 ky to 55 ky below the KPB (Fig. 2). Extreme event EE4 (347 ky pre-KPB) occurred near the base of C29r coincident with the onset of global climate warming (Fig. 2). Hg EE5 (283 ky pre-KPB) coincided with peak warming through EE6 (229 ky pre-KPB), which typically marks the zone CF2/CF1 boundary in many sequences analyzed. Decreasing Hg values and gradual cooling between 200 and 115 ky pre-KPB were temporarily interrupted by EE7 (180 ky pre-KPB). Allthough associated with high TOC, when normalized EE7 Hg/TOC is well below average (Fig. 2). We still consider EE7 as potentially valid Hg spike because of its presence in the Hor Hahar section of Israel where TOC is low (< 0.2 wt%, Fig. 5). EE8 (105 ky pre-KPB) and EE9 (72.5 ky pre-KPB) mark major Deccan eruption pulses and warming.

At 55–45 ky pre-KPB, climate rapidly cooled (temperature decrease of 3 °C) and warmed again between 45 and 25 ky pre-KPB. During this overall cool interval (55–25 ky pre-KPB), Hg input was low but variable apparently driven by very low Deccan CO_2 emissions (Fig. 2). In deep-sea sections, this cool event generally underlies the KPB due to a common erosion/hiatus during this time (Fig. 3) (Li and Keller 1998a; Punekar et al., 2014a; Keller et al., 2016; Mateo et al., 2017). Recently, some scientists interpreted the juxtaposition of this cooling and the mass extinction in deep-sea sections as evidence that Deccan volcanism ceased well prior to the KPB and the Chicxulub impact caused the global cooling and end-Cretaceous mass extinction (e.g., Sprain et al., 2019; Hull et al., 2020; Chiarenza et al., 2020). The expanded and complete Elles record challenges this interpretation.

Between 25 ky pre-KPB (cycle 1.5) and the KPB, rapid oscillations in Hg content, assigned to EE10 through EE20 culminate with the mass extinction (Fig. 2; Table A2). We infer that the associated massive volcanic eruptions, EE10 at 25 ky pre-KPB and EE11 at 12.5 ky pre-KPB, caused hyperthermal warming of 2.5–3.0 °C followed by temporal cooling of 1.5–2.0 °C. During the last ~4 ky pre-KPB, eruptions resumed with greater force and tempo in a series of larger extreme events (EE12 to EE20) in rapid succession ending in the mass extinction. Significant gypsum (Ca-sulfate) is present at and right above the KPB, which was probably formed by oxidation of pyrite and consequently accounts for part of the Hg enrichments (see section 4.2.3). Although the correlation between Hg and gypsum is low ($r = 0.27, n = 19$; Fig. 4, Fig. A9), there may still be some dependence of Hg on gypsum, particularly at the KPB.

We conclude this new evidence supports a link between late Maastrichtian warming in C29r and extreme mercury events in marine sequences. Furthermore, we show that the cooling, commonly believed to coincide with the KPB mass extinction, reflects a temporary lull in eruption rates between 55 and 25 ky prior to the KPB. This cooling underlies the KPB hiatus, which is ubiquitous in the deep-sea and marginal marine environmental records (Fig. 3). The complete KPB transition at Elles preserves evidence of extreme Deccan eruptive pulses that began during the last 25 ky pre-KPB and initiated hyperthermal warming that ended with the mass extinction (Fig. 2).

6. Testing the global distribution of Elles Hg extreme events

6.1. Introduction

If the Elles Hg extreme events are linked to major Deccan eruption pulses in India, they should be globally distributed in marine sediments. We tested this hypothesis in Israel based on Hg concentrations for the equivalent late Maastrichtian interval in the Hor Hahar section of the Negev (Fig. 1) which has very low TOC (< 0.2 wt%), except for some short intervals, and an average sedimentation rate of ~3.5 cm/ky for C29r compared with 4.7 cm/ky for Elles (Fig. 5). Lithology consists of marl, marly chalk and limestone, with shale above the KPB hiatus. Hg analysis were performed following the same methodology described in section 5.2.

6.2. Results

Hg analysis revealed a good correlation between Elles and Hor Hahar for extreme events EE3 to EE11. The average Hg concentration at Hor Hahar is 46 ppb compared with 35 ppb at Elles and most Hg extreme events are also higher than at Elles. Hg EE10 to EE11 correlate with the onset of hyperthermal warming at Elles, which abruptly ends at the well-documented KPB hiatus at Hor Hahar and other Negev and Sinai sections (Fig. 5) (Keller and Benjamini, 1991; Keller et al., 2002a; Keller, 2004; Adatte et al., 2005; Punekar et al., 2014b). The high Hg concentrations in the early Paleocene above the KPB hiatus coincide with high TOC (up to 1.9 wt%), yielding normalized values below average Hg/TOC.

The correlation between Elles and Hor Hahar is promising considering the sample spacing at Hor Hahar is variable ranging from 10 to 30-cm intervals for the late Maastrichtian and the sediment accumulation rate is lower. Higher resolution sampling could strengthen the correlation of extreme events between Tunisia and Israel and may also

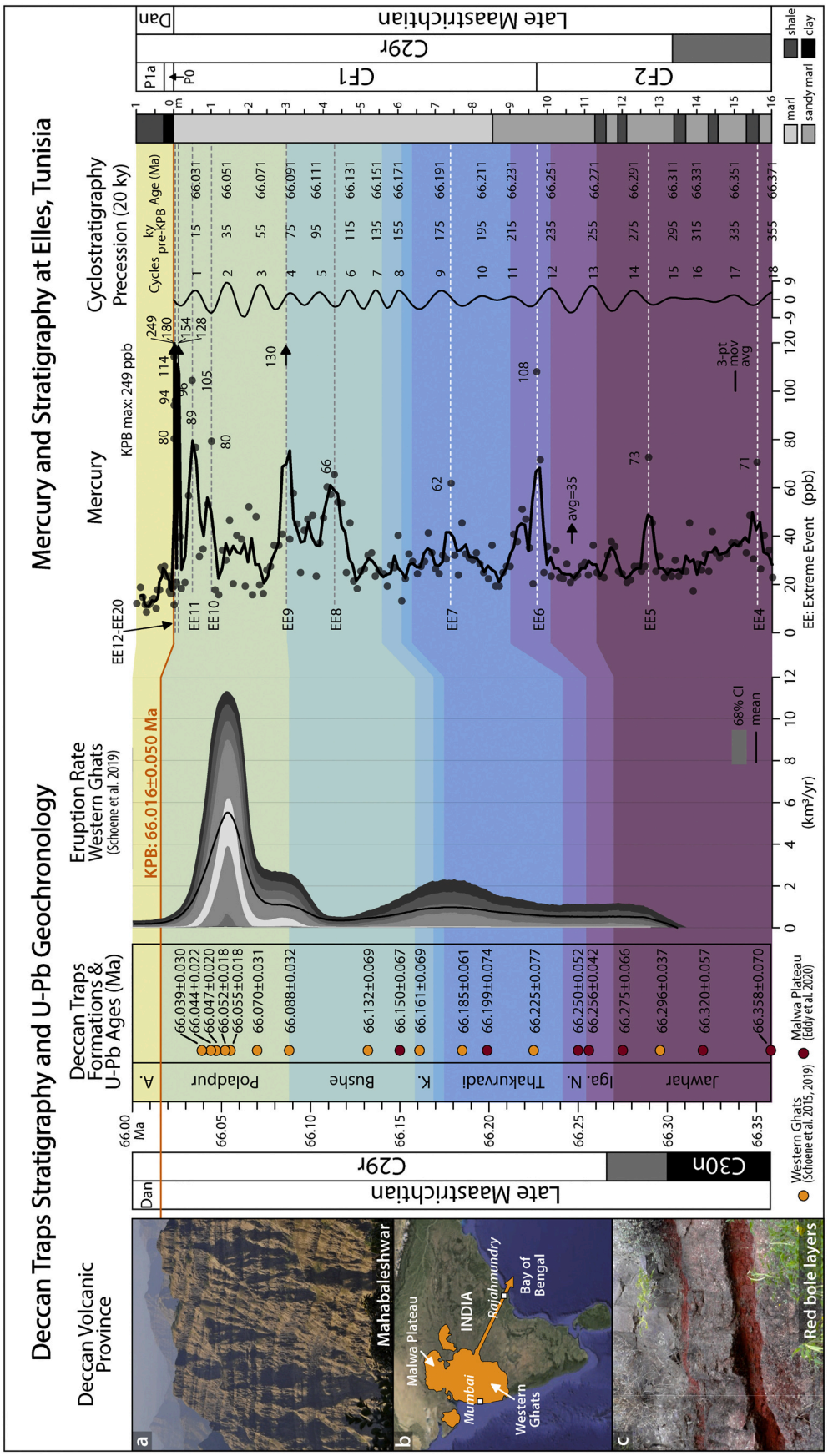

Fig. 6. Deccan Traps stratigraphy, geochronology and eruption rate estimates compared to high-resolution Hg data at the astronomically tuned Elles section in Tunisia. Note (1) the correlation between Deccan Traps U-Pb ages and Elles cyclostratigraphic ages and intervals of high Hg content at Elles reflect high Deccan eruption volumes; (2) the Poladpur Formation (66.016–66.088 Ma) reveals extremely high-volume eruptions supported by Hg loading at Elles that also indicates increasingly larger and more frequent eruptions during the last 25 ky of the Maastrichtian (there are no U-Pb ages in the top 23 ky below the KPB which affects the eruption rate model by shifting the largest pulse of eruptions below the 25 ky pre-KPB interval). U-Pb geochronologic uncertainties reported at the 95% C.I. and cyclostratigraphic ages at Elles reported with an uncertainty of ± 20 ky (one precession cycle). Deccan Traps U-Pb dates and KPB age at 66.016 ± 0.050 Ma from Schoene et al. (2015, 2019) and Eddy et al. (2020). Ma: millions of years ago, ky: thousands of years.

detect additional extreme events. However, even at this coarser sampling resolution, the presence of EE3 to EE11 in geographically disparate localities is compelling evidence for a global distribution of Hg, with a likely origin from the Deccan LIP. Thus, Hg proxy and Hg-stratigraphy are valuable correlation tools for linking extreme volcanic eruption events in marine sediments to LIP volcanism and, in this case, to the end-Cretaceous mass extinction at the KPB.

7. Elles age and Hg-stratigraphy correlated with Deccan volcanism

7.1. Introduction

We demonstrated Hg is an excellent proxy for Deccan volcanism in marine sediments at Elles, Tunisia, and Hor Hahar, Israel, with extreme eruption pulses linked to warming in coeval sediment samples (Figs. 2, 5). Mercury is thus not only a global proxy of Deccan volcanism but also an excellent global chemostratigraphic tool. Here we test whether Hg-stratigraphy at Elles can be linked to the Deccan eruption history and U-Pb geochronology for C29r below the KPB based on Elles cyclostratigraphy age control and Hg extreme events (EE4 to EE19) (Fig. 6, Fig. A5). If this correlation can be reasonably accomplished, then the global Hg EEs are demonstrably linked to Deccan eruption pulses, climate and environmental changes.

7.2. Review of Deccan eruption pulses

The main phase of Deccan volcanism is interpreted to have occurred in three major phases based on paleomagnetic data (Chenet et al., 2007, 2008, 2009) and four major pulsed eruption events based on stratigraphic age modeling of U-Pb zircon geochronologic data (Schoene et al., 2019) (Fig. 6, Fig. A5). Pulse-1 is interpreted as coinciding with the long-term global warming in C29r, which has long been attributed to Deccan volcanism as early as 1998 (Li and Keller 1998a) and is now supported by the Elles sequence spanning Hg EE4 through EE9 (345–72.5 ky pre-KPB) (Fig. 2). The most intense pulse, pulse-2, corresponds to the eruption of Deccan's Poladpur Formation, that Schoene et al. (2019) propose to have started within tens of ky prior to the KPB, as dated by Clyde et al. (2016) using U-Pb geochronology in the Denver Basin, Colorado, USA. Pulse-3 occurred about 100 ky after the KPB mass extinction and the last pulse, pulse-4, occurred at or close to the base of C29n (Chenet et al., 2009; Schoene et al., 2019), potentially correlative with climate warming of Dan-C2 and preceding the onset of full biotic recovery.

An alternative eruption record was presented in Sprain et al. (2019) based on $^{40}Ar/^{39}Ar$ geochronology. These authors advocated for a more constant eruption rate with a step change to higher rates at the KPB boundary. However, the precision of these measurements is not sufficient to test for the existence of the eruptive pulses inferred from the U-Pb data (Schoene et al., 2020). Further discussion of these two datasets can be found in Appendix A (Section A.4).

7.3. Comparison between Deccan U-Pb ages and Elles Hg EEs

Deccan geochronology based on U-Pb zircon ages are from the Western Ghats (Schoene et al., 2015, 2019) and Malwa Plateau (Eddy et al., 2020) with reported uncertainties at the 95% C.I. (see below). Cyclostratigraphy is based on precession cycles at Elles with an assumed uncertainty of one precession cycle (± 20 ky). In this study, we restrict this correlation to C29r below the KPB. Table A2 lists the Deccan U-Pb zircon ages and cyclostratigraphy precession cycles, ages and Hg extreme events relative to a KPB age of 66.016 Ma.

Recently, the two oldest U-Pb zircon ages from the main Deccan Volcanic Province were dated 66.358 ± 0.070 Ma and 66.320 ± 0.057 Ma (342 ky and 304 ky pre-KPB, respectively) in C30n of the Narmada Formation from the Malwa Plateau, which is equivalent to the Jawhar Formation of the Western Ghats (Eddy et al., 2020) (Fig. 6; Table A2). These ages are within uncertainties of Elles Hg EE4 at 66.363 Ma and EE5 66.299 Ma (347 ky and 283 ky pre-KPB, respectively) and likely mark the onset of Deccan induced climate warming near magnetic reversal C30n/C29r (Figs. 2, 6; Table A2). In the Western Ghats, the oldest volcanic unit is the Jawhar Formation deposited through the C30n/C29r transition (Chenet et al., 2009; Schoene et al., 2015), and the oldest U-Pb zircon age is 66.296 ± 0.037 Ma (280 ky pre-KPB) from a lava interpreted as having transitional polarity (Schoene et al., 2015, 2019). In the Malwa Plateau, ages of 66.320 ± 0.057 Ma and 66.275 ± 0.066 Ma (304 ky and 259 ky pre-KPB, respectively) appear to correlate with the middle and top Jawhar Formation in the Western Ghats (Eddy et al., 2020) and with cycles 15 and 13 at Elles associated with warm/cool fluctuations (Fig. 6).

The younger Malwa Plateau U-Pb zircon ages 66.256 ± 0.042 Ma and 66.250 ± 0.052 Ma (241 ky and 234 ky pre-KPB, respectively) from the Manpur Formation are correlative with Igatpuri and Neral Formations in the Western Ghats. These ages correlate with Elles cycles ~12.5 at 66.261 Ma and 12 at 66.251 Ma (245 ky and 235 ky pre-KPB, respectively) associated with cooling (Fig. 6; Table A2). The Neral Formation appears to correlate with Elles EE6 (229 ky pre-KPB), which marks the biostratigraphic zone CF2/CF1 boundary and maximum warming (Figs. 2, 5). Two U-Pb ages from the lower and upper Thakurvadi Formation at 66.225 ± 0.077 Ma and 66.185 ± 0.061 (209 ky and 169 ky pre-KPB, respectively) in the Western Ghats span cycles 11 to 8.5 at Elles linked to warm/cool fluctuations. The middle Thakurvadi Formation age, correlative to the Manpur Formation of the Malwa Plateau at 66.199 ± 0.074 Ma (183 ky pre-KPB), correlates with Elles EE7 at 66.195 Ma (180 ky pre-KPB) and warming (Fig. 6; Table A2).

The Khandala Formation U-Pb age at 66.161 ± 0.069 Ma (145 ky pre-KPB) correlates with Elles cycle ~7.5 at 66.161 Ma (145 ky pre-KPB) and gradual cooling (Fig. 6; Table A2). In the lower Bushe Formation two U-Pb ages at 66.150 ± 0.067 Ma and 66.132 ± 0.069 Ma (134 ky pre-KPB, Malwa Manpur equivalent, and 116 ky pre-KPB, respectively) correlate with Elles cycles 7 and 6 at 66.151 Ma and 66.131 Ma, respectively, associated with low Hg concentrations and a gradual cooling trend (Figs. 2, 6; Table A2).

The major Hg EE8 and cycle ~5.5 (66.121 Ma, 105 ky pre-KPB) correlate with the Bushe Formation. The Bushe/Poladpur transition U-Pb age at 66.088 ± 0.032 Ma (72 pre-KPB) correlates with EE9, cycles 4–3 at Elles (66.089 Ma, 72.5 ky pre-KPB) and rapid climate warming (Figs. 2, 6; Table A2). After this warm event, climate cooled rapidly and remained cool between 45 and 25 ky pre-KPB, during a time of low Hg concentrations that reflect low magnitude volcanic eruptions. Five U-Pb ages mark this cool interval in the Deccan Western Ghats at 66.070 ± 0.031 Ma to 66.044 ± 0.022 Ma (54 to 28 ky pre-KPB) (Fig. 6; Table A2). The last U-Pb age from the Poladpur Formation is at 66.039 ± 0.030 Ma and 23 ky pre-KPB, near the onset of the hyperthermal warming. However, all of these Poladpur ages are within error margins of the estimated KPB age at 66.016 ± 0.050 Ma. In contrast, Elles cyclostratigraphy ages for Hg EE10 to EE20 span the last 25 ky (1 m) below the KPB correlative with hyperthermal warming as described in section 5.4 (Fig. 2; Table A2).

8. Discussion

8.1. Global climate, volcanism and the mass extinction

The direct link between Hg anomalies and climate change based on $\delta^{18}O$ of benthic foraminifera at Elles, Tunisia, is evidence for Deccan volcanism's effect on global climate. This effect is particularly evident by the long-term warming from the base of C29r (350 ky pre-KPB) to short-term cooling between 72 and 26 ky pre-KPB, followed by hyperthermal warming during the last 25 ky, ending at the KPB with the mass extinction (Fig. 7). Extreme Deccan eruption events (EE4 to EE9)

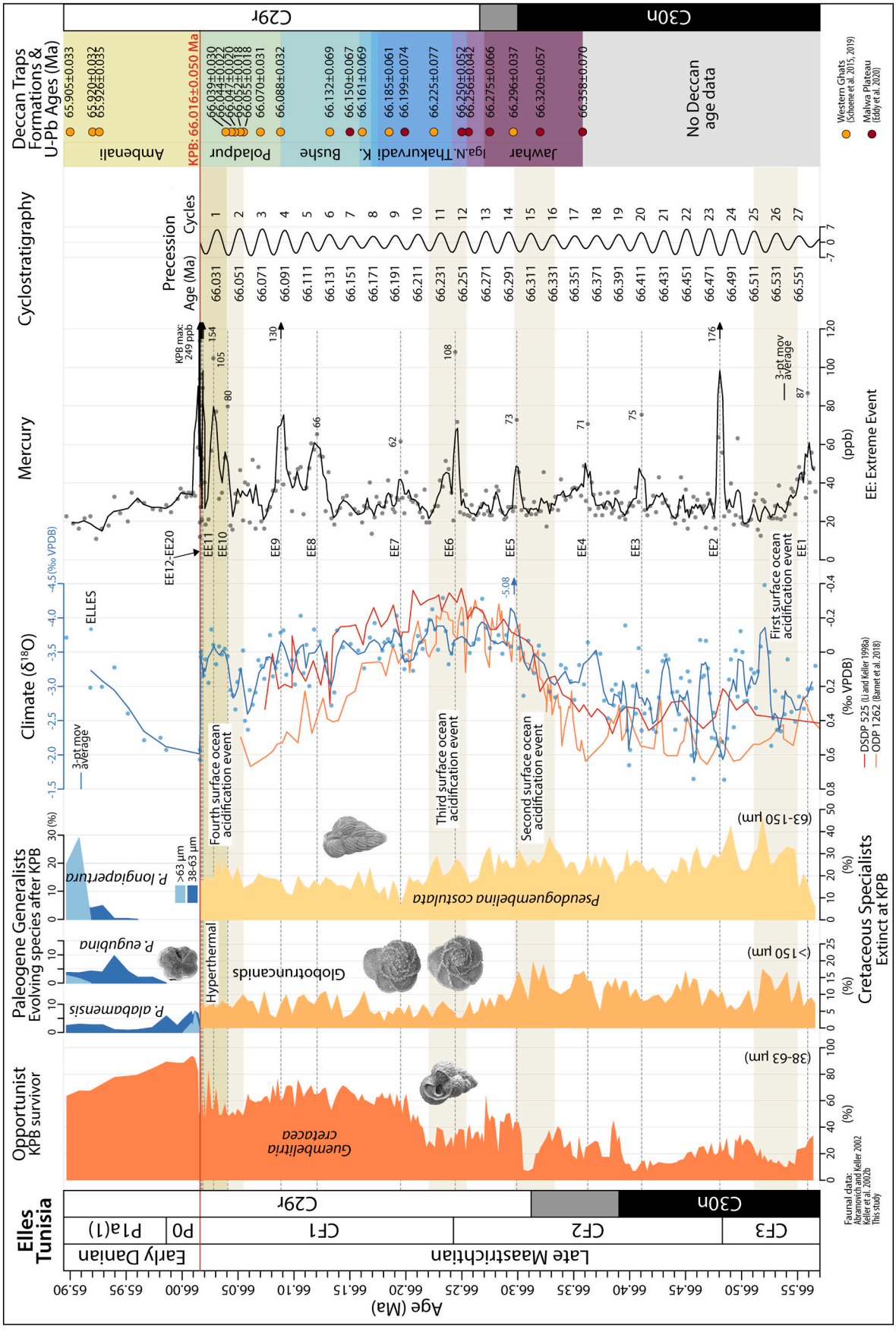

Fig. 7. High-resolution planktic foraminifera and relative abundances, $\delta^{18}O$ and Hg data at the astronomically tuned Elles section in Tunisia and comparison with $\delta^{18}O$ data at Sites 525A and 1262, Deccan Traps stratigraphy and geochronology. Note the direct link between Hg anomalies and $\delta^{18}O$ at Elles (and at Sites 525A and 1262) demonstrates the effect of Deccan volcanism on global climate; the rapid increase in Hg loading (paroxysmal Deccan eruptions) correlates to hyperthermal warming and surface ocean acidification during the last 25 ky pre-KPB, as also observed in C30n, lower C29n (CF2 and CF2/CF1). Increased stress on marine life through the late Maastrichtian (increased relative abundance of disaster opportunist species, decreased specialist species) reached maximum during the last 25 ky pre-KPB and ended with the mass extinction. KPB age at 66.016 ± 0.050 Ma and Deccan Traps U-Pb dates from Schoene et al. (2015, 2019) and Eddy et al. (2020). Uncertainty in cyclostratigraphic ages: ± 20 ky (one precession cycle). Ma: millions of years ago, ky: thousands of years.

at ~40–50 ky intervals appear to have driven the long-term warming. Still puzzling is the quasi-periodicity of these Hg extreme events. A sampling artifact can be ruled out because the same extreme events are observed in Israel and other localities (Fig. 5). Perhaps this is a fractal eruption pattern of LIP events (Grasby et al., 2020). The following 46 ky period of short-term global cooling correlates with overall low Hg concentrations (< 20 ppb) and hence low atmospheric CO_2 input from Deccan eruptions that results in cooling.

8.2. Hyperthermal KPB event

Hyperthermal warming suddenly ended the short-term cooling 25 ky pre-KPB at Elles, with accelerating Hg extreme events (EE10 to EE20) correlated with the largest eruption pulse of the Deccan LIPs at the end of the Poladpur Formation (Fig. 6) (Schoene et al., 2019). At Elles, Hg EE10-EE11 are coeval with the onset of hyperthermal warming that continued through Hg EE12-EE20, spanning the last 25 ky of the Maastrichtian and ending with the mass extinction at the KPB (Figs. 2, 7). This hyperthermal warming was also observed at Hor Hahar, Israel, where Hg EE10-EE11 are present and mark the onset of this event, but erosion/hiatus spans EE12-EE20, the KPB and part of the early Danian (Fig. 5). Further evidence of this end-Cretaceous hyperthermal catastrophe is likely to be discovered in continental shelf environments with high sediment accumulation rates and analyses based on very high sample resolution (1 cm to 5 cm intervals).

Previous discoveries of the mass extinction between trans-India lava flows in the Rajamundry quarries (Keller et al., 2008) and particularly between four of these lava flows in deep cores from the Krishna-Godavari Basin (Keller et al., 2011, 2012) linked the mass extinction directly to the major Deccan eruptions pulse across the KPB (Schoene et al., 2019). Hg stratigraphy at Elles now further refines the mass extinction between the last five Hg extreme events (EE16-EE20) of the hyperthermal warming, which indicate the mass extinction occurred rapidly over ≤1000 years (Fig. 7). This time estimate is in good agreement with time limits set to eruption pulses using paleomagnetic directions and secular variations suggesting duration of only one century for each of the largest lava flows (Chenet et al., 2009). The cause(s) for these rapid and extreme eruption events is still speculative, but not restricted to the Deccan LIPs at the time of the end-Cretaceous mass extinction. Siberian Trap eruptions may have been similar and driven repeated global toxic stress on marine and terrestrial environments (Grasby et al., 2020). Deccan Traps accelerated Hg extreme events and hyperthermal warming leading up to the mass extinction support this interpretation and so do the trans-India lava flows that ended with the mass extinction.

8.3. KPB hiatus

The long-term climate pattern and short-term cooling preceding the end-Cretaceous mass extinction observed at Elles is also present in the South Atlantic DSDP Sites 525 and 528, ODP Sites 690, 1209, 1262 and 1267 (Keller, 1993; Li and Keller 1998a; Westerhold et al., 2008; Barnet et al., 2018). Missing in deep-sea sites is the hyperthermal warming leading up to the mass extinction due to a KPB hiatus (Figs. 3, 7). Hiatuses are ubiquitous in deep-sea sections at depths of 1000–4000 m, because sediment deposition is extremely slow (< 1 cm/ky) and exposure to major current circulation results in frequent erosion/hiatuses, particularly during intensified currents driven by global cooling. In contrast, continental shelf deposition, such as at Elles (depth of 100–150 m), has high sediment deposition rates (~4.7 cm/ky) and are relatively protected from major currents. The shortest deep-sea hiatuses span from the early Danian to the short cool event 45–26 ky below the KPB, thus missing the hyperthermal and the mass extinction horizon. This hiatus has been documented in deep-sea localities from the Atlantic, Pacific and Indian Oceans (Li and Keller 1998a; Keller et al., 2013, 2016; Thibault and Husson, 2016; Punekar et al., 2014a, 2016; Mateo et al., 2016, 2017; Font et al., 2018).

Evaluation of the short-term environmental changes across the end-Cretaceous mass extinction and hyperthermal event thus necessitates high-resolution quantitative, biostratigraphic age control to document the continuity of species populations or sudden disappearance during prime population abundances due to a hiatus. Hg stratigraphy is the new tool that adds an independent proxy to interpret the nature and cause of the mass extinction linked to the Deccan LIP.

Recently, the assumption of a complete KPB record in deep sea sites, including South Atlantic localities, led to claims that the mass extinction occurred during the short-term global cooling that underlies the KPB hiatus. In the absence of major Hg concentrations, this cooling was attributed to the Chicxulub impact as prime cause for the mass extinction (e.g., Henehan et al., 2016; Hull et al., 2020; Chiarenza et al., 2020). This scenario is not supported in complete KPB sections such as Elles, Tunisia, where climate cooling abruptly ended prior to the hyperthermal warming and major Deccan eruption pulse (EE10-EE20) that ended in the end-Cretaceous mass extinction.

8.4. Biotic crisis

The end-Cretaceous mass extinction story can be divided into two parts: (1) the biotic turnover during a long period of environmental stress (~300 ky) caused by Deccan volcanism-induced climate warming; and (2) the tipping point and sudden mass extinction during the last 25 ky pre-KPB correlated with the largest Deccan eruption pulse, hyperthermal warming and ocean acidification. Paleontologists have long known the gradual extinction pattern from the fossil record and often interpreted the sudden mass extinction as the end-result of a gradually deteriorating environment due to volcanism, climate and sea-level changes, greenhouse warming accompanied by fluctuating anoxia and nutrient dynamics leading to the decimation of marine organisms (Benton, 1995; Hallam and Wignall, 1997; House, 2002). Since 1980, the sudden mass extinction has been solely attributed to the Chicxulub impact (Alvarez et al., 1980; review in Schulte et al., 2010). But recent discoveries have added more details and complexity to the long-term biotic turnover and the sudden mass extinction, linking both directly to Deccan volcanism induced climate change and ocean acidification but at starkly different rates and tempo (review in Punekar et al., 2014a; Keller et al., 2018).

In this study, the biotic turnover and mass extinction are evaluated based on planktic foraminifera from Elles, Tunisia, which contains the most complete records for the late Maastrichtian and KPB transition known worldwide (Abramovich and Keller, 2002; Punekar et al., 2014a).

8.4.1. The biotic turnover

In low and middle latitude marine environments planktic foraminiferal diversity averaged about 65 species (e.g., Li and Keller, 1998b; Abramovich and Keller, 2002). About 2/3 of these assemblages (44 species) were large, complex and ornate thick-walled species. Twenty-seven of these species belong to the most ornate and diverse group, the globotruncanids, adapted to normal pH, warm temperature, normal salinity, oxygen and nutrient conditions. At Elles, high-stress conditions during the late Maastrichtian (66.550–66.291 Ma) already reduced the total abundance of globotruncanids to 5–15%, compared to 35% in the interval prior to the first surface ocean acidification event (Fig. 7). The second and third acidification events coincided with the onset of Deccan-induced long-term climate warming and peak warming, respectively, when globotruncanid populations decreased to 5–10% (Fig. 7). Planktic foraminifera thus reveal long-term high-stress conditions endangered all environmentally sensitive species (66%) during the duration of Deccan eruptions and climate warming prior to the KPB but caused no extinctions.

The remaining third of the assemblages (22 species) were smaller species with simple morphologies, less ornamentation and thin shells

adaptable to variable environmental conditions across latitudes (e.g., Li and Keller, 1998b; Abramovich and Keller, 2002). Biserial species dominated in this group, including the surface dweller *Pseudoguembelina costulata* and *P. costellifera*. At Elles, *P. costulata* decreased in abundance after the third acidification event (Fig. 7).

8.4.2. Disaster opportunist Guembelitria

Guembelitria cretacea is known as disaster opportunist and sole long-term survivor of the end-Cretaceous mass extinction. This species adapted and thrived in high-stress environments and nutrient-rich surface waters by reduced species size (Lilliput effect), thin shells and rapid reproduction rates (Keller and Abramovich, 2009; Abramovich et al., 2010; Ashckenazi-Polivoda et al., 2014). *Guembelitria cretacea* is generally only analyzed in the > 63 μm size fraction when it thrived after the mass extinction. However, this species also thrived during the late Maastrichtian high-stress environment by species dwarfing from > 63 μm to 38–63 μm size fraction, marking the *Guembelitria* Lilliput population which yields a new proxy for high-stress conditions associated with Deccan volcanism preceding the mass extinction. In this study we analyzed the *Guembelitria* Lilliput population (38-63 μm) for the first time from the late C30n through C29r across the KPB and into the early Danian. The first indication of really high-stress conditions was marked by abundant (60%) *Guembelitria cretacea* in cycle ~9.5, 165 ky pre-KPB coincident with EE7 (early zone CF1) (Fig. 7). However, higher stress conditions likely prevailed already in the preceding maximum warming and third acidification event, where reduced *Guembelitria* populations resulted from enhanced shell fragmentation due to dissolution effects. After the third acidification event, environmental stress steadily increased with high *Guembelitria* abundances between 60 and 70%, and decreased abundances of all larger species. *Guembelitria* abundances decreased to 50% during the short-term global cooling. Maximum stress began with the onset of hyperthermal warming and acidification spanning the last 25 ky pre-KPB (Fig. 7). This interval shows significantly reduced *Guembelitria* abundances due to acidification and fragmentation of thinner shells, but some high peaks (80%) prevailed (Fig. 7). Above the KPB, *Guembelitria cretacea* rapidly regained larger sizes (> 63 μm) and dominated early Danian planktic foraminiferal populations by nearly 100%. During this time *Guembelitria* diversified and evolved into the new Paleocene fauna (Fig. 7).

8.4.3. Sudden mass extinction

During the last 25 ky before the KPB, a paroxysmal eruption pulse resulted in a sudden climate change to hyperthermal warming and increasingly acidic and toxic oceans (Fig. 7). The large, specialized planktic foraminiferal species (66%), already endangered by the preceding ~300 ky of environmental stress, reached threshold conditions and went extinct far more rapidly than previously estimated from environmental factors. The extinction climax was reached during the four to five largest Hg extreme events (EE16-EE20) at the end of the largest Deccan eruption pulse during ≤1000 years at the end of the Cretaceous. The smaller environmentally more tolerant species severely reduced populations and survived for 50–100 ky into the early Danian. The sole long-term survivor and disaster opportunist *Guembelitria cretacea* thrived and gave rise to the newly evolved early Danian species.

In India, the mass extinction was previously documented between three to four Deccan lava flows that traversed > 1000 km from the main Deccan Volcanic Province to the Bay of Bengal (Keller et al., 2008, 2011, 2012). These lava flows correlate to the Hg extreme events that sealed the mass extinction at Elles (EE15-EE20). Oxygen stable isotopes and Hg-stratigraphy revealed a temporally complete sequence linked to Deccan volcanism via U-Pb dating and cyclostratigraphy. Thus, Elles serves as an ideal model to assess the global nature, rate and tempo of the end-Cretaceous mass extinction as well as to evaluate the timing and contribution of the Chicxulub impact relative to Deccan volcanism in this major biotic crisis.

9. Summary and conclusions

The Elles section in Tunisia is the auxiliary GSSP to the El Kef section and has the most complete late Maastrichtian sedimentary record and high sedimentation rate (~4.7 cm/ky) in a middle shelf environment at 100–150 m paleodepth. We chose this section to test the global mercury (Hg) fallout as a potential proxy for major Deccan eruptions and global chemostratigraphic correlation tool linking KPB sequences to Deccan volcanism. The ultimate goal was to evaluate Deccan volcanism's direct role in long-term climate warming during C29r and the hyperthermal during the last 25 ky preceding the KPB and how these climate changes affected both long-term biotic turnover and the nature and tempo of the mass extinction. Results demonstrate Deccan volcanism's long-term detrimental effects on marine life and reveal paroxysmal eruptions, toxicity and ocean acidification as a critical driver of the rapid mass extinctions. We arrived at this conclusion by synthesizing a multitude of analyses that are summarized below.

1. At Elles we successfully analyzed orbital cyclostratigraphy for maximum age control and correlation with high-resolution U-Pb zircon dating of the Deccan Traps (Schoene et al., 2019) (Fig. 2).
2. We analyzed sediments for Hg concentrations in the Elles section at ~1.25-ky (10-cm) intervals for the 525 ky pre-KPB. Results reveal an elevated Hg background that we attribute to volcanic activity and punctuated Hg extreme enrichments (EE1 to EE9) that we interpret as representing large eruption events (Fig. 2).
3. Hg concentrations during the last 25 ky pre-KPB, analyzed at higher resolution (0.5 cm, 1 cm to 5 cm intervals), revealed extreme events (EE10 to EE20) linked to paroxysmal eruptions, temporally related to hyperthermal warming and the mass extinction (EE16 to EE20) (Figs. 2, 7).
4. Carbon and oxygen stable isotopes ($\delta^{13}C$, $\delta^{18}O$) and Hg concentrations in coeval samples demonstrate the correlation between long-term climate warming and elevated background Hg concentrations (35 ppb), with warm peaks further associated with EE4-EE9 (Fig. 2). This correlation supports the direct link between volcanism and climate warming.
5. Paroxysmal Deccan eruptions during the last 25 ky pre-KPB coincide with inferred hyperthermal warming and the mass extinction (Fig. 7).
6. We tested the reliability of Hg concentrations at Elles by analyzing the Hor Hahar sequence in Israel. The Hg curves for both locations suggest that the Hg concentrations reflect global processes, supporting a volcanic origin (Fig. 5).
7. We correlated Elles cyclostratigraphy and Hg stratigraphy results with Deccan Traps stratigraphy and U-Pb geochronology (Fig. 6). Results demonstrate a direct link between major Deccan volcanic eruptions in India and Hg spikes in marine sediments correlative with climate warming peaks.
8. We evaluated the biotic response to Deccan volcanism based on climate warming and Hg stratigraphy (Fig. 7). Results demonstrate increasingly high-stress environments during the long-term climate warming in C29r, and rapid mass extinction during paroxysmal eruptions and hyperthermal warming during the last 25 ky of the Cretaceous.

We conclude that the results of this study at Elles, Tunisia, reveal pulsed Deccan volcanic eruptions identified based on Hg concentrations in sediments that caused long-term climate warming and biotic turnover but no significant species extinction. However, the paroxysmal eruptions during the last 25 ky caused hyperthermal warming, ocean acidification and toxicity that exceeded threshold conditions for life leading to the rapid mass extinction during the most extreme events (EE16 to EE20) spanning ≤1000 years at the end of the Cretaceous. Evidence of these extreme events is manifest in the longest known lava flows, > 1000 km, that originated in the main Deccan province and

spanned across India. The extremely rapid mass extinction was first documented in sediments between the four longest lava flows in cores drilled by India's Oil and Natural Gas Corporation (ONGC) and now confirmed based on Hg extreme events at Elles, Tunisia.

The sum total of the current studies demonstrates extreme event Deccan eruptions caused long-term climate warming in C29r and short-term hyperthermal warming during the last 25 ky prior to the end-Cretaceous mass extinction at the KPB. These observations strongly support Deccan volcanism as main contributor to climate change and the end-Cretaceous mass extinction, and call for a re-evaluation of the relative roles of both the Chicxulub impact and Deccan volcanic eruptions in this major biotic crisis.

Data and materials availability

All data and supplementary materials are available in Appendix A.

Author Contributions

Gerta Keller: Conceptualization; Data Curation; Formal analysis; Funding acquisition; Investigation; Methodology; Project administration; Resources; Supervision; Validation; Writing – original draft; Writing – review & editing. **Paula Mateo:** Conceptualization; Data Curation; Formal Analysis; Investigation; Project administration; Visualization; Writing – original draft; Writing – review & editing. **Johannes Monkenbusch and Nicolas Thibault:** Formal analysis; Investigation; Methodology; Validation; Visualization; Writing – review & editing. **Jahnavi Punekar:** Investigation; Resources; Writing – review & editing. **Jorge E. Spangenberg:** Investigation; Methodology; Validation; Writing – review & editing. **Sigal Abramovich and Sarit Ashckenazi-Poliveda:** Investigation; Resources; Writing – review & editing. **Blair Schoene, Michael P. Eddy and Kyle M. Samperton:** Formal analysis; Investigation; Methodology, Resources; Validation; Writing – review & editing. **Syed F.R. Khadri:** Investigation; Resources. **Thierry Adatte:** Investigation; Resources; Writing – review & editing.

Declaration of Competing Interest

Authors declare no competing interests.

Acknowledgements

We are grateful to the reviewers, Vincent Courtillot and Steve Grasby, for their insightful comments and suggestions to improve this paper. We thank Renee Delamater-Droungas and Udit Basu for help with mercury analyses, and Brian Gertsch for the Elles trace element data. This research was supported by the Geosciences Department at Princeton University [Tuttle and Scott grants] and the Carlsberg Foundation [CF16-0457]. Lawrence Livermore National Laboratory is operated by Lawrence Livermore National Security, LLC, for the U.S. Department of Energy, National Nuclear Security Administration under Contract DE-AC52-07NA27344. This paper is LLNL contribution LLNL-JRNL-811397. University of Copenhagen, Carlsbergfondet grant CF16-0457.

Appendix A. Supplementary data

Supplementary data to this article can be found online at https://doi.org/10.1016/j.gloplacha.2020.103312.

References

Abramovich, S., Keller, G., 2002. High stress late Maastrichtian Paleoenvironment in Tunisia: Inference from planktic foraminifera. Paleogeogr. Paleoclimatol. Paleoecol. 178, 145–164. https://doi.org/10.1016/S0031-0182(01)00394-7.

Abramovich, S., Yovel-Corem, S., Almogi-Labin, A., Benjamini, C., 2010. Global climate change and planktic foraminiferal response in the Maastrichtian. Paleoceanography 25, PA2201. https://doi.org/10.1029/2009PA001843.

Adatte, T., Keller, G., Stueben, D., Harting, M., Kramar, U., Stinnesbeck, W., Abramovich, S., Benjamini, C., 2005. Late Maastrichtian and K/T paleoenvironment of the eastern Tethys (Israel): mineralogy, trace and platinum group elements, biostratigraphy and faunal turnovers. B. Soc. Geol. Fr. 176, 37–55. https://doi.org/10.2113/176.1.37.

Aiuppa, A., Inguaggiato, S., McGonigle, A.J.S., O'Dwyer, M., Oppenheimer, C., Padgett, M.J., Rouwet, D., Valenza, M., 2005. H_2S fluxes from Mt. Etna, Stromboli, and Vulcano (Italy) and implications for the sulfur budget at volcanoes. Geochim. Cosmochim. Ac. 69, 1861–1871. https://doi.org/10.1016/j.gca.2004.09.018.

Allard, P., Carbonnelle, J., Métrich, N., Loyer, H., Zettwoog, P., 1994. Sulphur output and magma degassing budget of Stromboli volcano. Nature 368, 326–330. https://doi.org/10.1038/368326a0.

Alvarez, L.W., Alvarez, W., Asaro, F., Michel, H.V., 1980. Extraterrestrial cause for the Cretaceous-Tertiary extinction. Science 208, 1095–1108. https://doi.org/10.1126/science.208.4448.1095.

Amos, H.M., Jacob, D.J., Kocman, D., Horowitz, H.M., Zhang, Y., Dutkiewicz, S., Horvat, M., Corbitt, E.S., Krabbenhoft, D.P., Sunderland, E.M., 2014. Global biogeochemical implications of mercury discharges from rivers and sediment burial. Environ. Sci. Technol. 48, 9514–9522. https://doi.org/10.1021/es502134t.

Andren, A.W., Harriss, R.C., 1975. Observations on the association between mercury and organic matter dissolved in natural waters. Geochim. Cosmochim. Ac. 39, 1253–1258. https://doi.org/10.1016/0016-7037(75)90132-5.

Ashckenazi-Polivoda, S., Rak, C., Almogi-Labin, A., Zsolt, B., Ovadia, O., Abramovich, S., 2014. Paleoecology of the K-Pg mass extinction survivor Guembelitria (Cushman): isotopic evidence from pristine foraminifera from Brazos River, Texas (Maastrichtian). Paleobiology 40, 24–33. https://doi.org/10.1666/13317.

Barnet, J.S., Littler, K., Kroon, D., Leng, M.J., Westerhold, T., Röhl, U., Zachos, J.C., 2018. A new high-resolution chronology for the late Maastrichtian warming event: establishing robust temporal links with the onset of Deccan volcanism. Geology 46, 147–150. https://doi.org/10.1130/G39771.1.

Beane, J.E., Turner, C.A., Hooper, P.R., Subbarao, K.V., Walsh, J.N., 1986. Stratigraphy, composition and form of the Deccan basalts, Western Ghats, India. Bull. Volcanol. 48, 61–83. https://doi.org/10.1007/BF01073513.

Benton, M.J., 1995. Diversification and extinction in the history of life. Science 268, 52–58. https://doi.org/10.1126/science.7701342.

Bond, D.P.G., Grasby, S.E., 2017. On the causes of mass extinctions. Palaeogeogr. Palaeoclimatol. Palaeoecol. 478, 3–29. https://doi.org/10.1016/j.palaeo.2016.11.005.

Bond, D.P.G., Wignall, P.B., 2014. Large Igneous Provinces and mass extinctions: An update. In: Keller, G., Kerr, A.C. (Eds.), Volcanism, Impacts, and Mass Extinctions: Causes and Effects. Geol. Soc. Am, vol. 505. pp. 29–55. https://doi.org/10.1130/2014.2505(02).

Bouffard, A., Amyot, M., 2009. Importance of elemental mercury in lake sediments. Chemosphere 74, 1098–1103. https://doi.org/10.1016/j.chemosphere.2008.10.045.

Bower, J., Savage, K.S., Weinman, B., Barnett, M.O., Hamilton, W.P., Harper, W.F., 2008. Immobilization of mercury by pyrite (FeS_2). Environ. Pollut. 156, 504–514. https://doi.org/10.1016/j.envpol.2008.01.011.

Brumsack, H.J., 1986. The inorganic geochemistry of Cretaceous black shales (DSDP leg 41) in comparison to modern upwelling sediments from the Gulf of California. In: Summerhayes, C.P., Shackleton, N.J. (Eds.), North Atlantic Palaeoceanography. Geol. Soc. Spec. Publ, vol. 21. pp. 447–462. https://doi.org/10.1144/GSL.SP.1986.021.01.30.

Charbonnier, G., Adatte, T., Foellmi, K., Suan, G., 2020. Effect of intense weathering and post-depositional degradation of organic matter on Hg sequestration in organic rich sediments and its implications for deep-time investigations. Geochem. Geophys. Geosyst. 21https://doi.org/10.1029/2019GC008707. e2019GC008707.

Chenet, A.L., Quidelleur, X., Fluteau, F., Courtillot, V., Bajpai, S., 2007. ^{40}K–^{40}Ar dating of the Main Deccan Large Igneous Province: further evidence of KTB age and short duration. Earth Planet. Sci. Lett. 263, 1–15. https://doi.org/10.1016/j.epsl.2007.07.011.

Chenet, A.-L., Fluteau, F., Courtillot, V., Gérard, M., Subbarao, K.V., 2008. Determination of rapid Deccan eruptions across the Cretaceous-Tertiary boundary using paleomagnetic secular variation: results from a 1200-m-thick section in the Mahabaleshwar escarpment. J. Geophys. Res. 113, B04101. https://doi.org/10.1029/2006JB004635.

Chenet, A.-L., Courtillot, V., Fluteau, F., Gerard, M., Quidelleur, X., Khadri, S.F.R., Subbarao, K.V., Thordarson, T., 2009. Determination of rapid Deccan eruptions across the Cretaceous-Tertiary boundary using paleomagnetic secular variation: 2. Constraints from analysis of eight new sections and synthesis for a 3500-m-thick composite section. J. Geophys. Res. 114https://doi.org/10.1029/2008JB005644. B06103.

Chiarenza, A.A., Farnsworth, A., Mannion, P.D., Lunt, D.J., Valdes, P.J., Morgan, J.V., Allison, P.A., 2020. Asteroid impact, not volcanism, caused the end-Cretaceous dinosaur extinction. P. Natl. Acad. Sci. USA 117, 17084–17093. https://doi.org/10.1073/pnas.2006087117.

Clyde, W.C., Ramezani, J., Johnson, K.R., Bowring, S.A., Jones, M.M., 2016. Direct high-precision U–Pb geochronology of the end-Cretaceous extinction and calibration of Paleocene astronomical timescales. Earth Planet. Sci. Lett. 452, 272–280. https://doi.org/10.1016/j.epsl.2016.07.041.

Courtillot, V., 1999. Evolutionary Catastrophes: The Science of Mass Extinction. Cambridge University Press, Cambridge.

Courtillot, V.E., Renne, P.R., 2003. On the ages of flood basalt events. Compt. Rendus Geosci. 335, 113–140. https://doi.org/10.1016/S1631-0713(03)00006-3.

Cranston, R.E., Buckley, D.E., 1972. Mercury pathways in a river and estuary. Environ. Sci. Technol. 6, 274–278. https://doi.org/10.1021/es60062a007.

Dessert, C., Dupré, B., Gaillardet, J., François, L.M., Allegre, C.J., 2003. Basalt weathering laws and the impact of basalt weathering on the global carbon cycle. Chem. Geol. 202, 257–273. https://doi.org/10.1016/j.chemgeo.2002.10.001.
Eddy, M.P., Schoene, B., Samperton, K.M., Keller, G., Adatte, T., Khadri, S.F., 2020. U-Pb zircon age constraints on the earliest eruptions of the Deccan large Igneous Province, Malwa Plateau, India. Earth Planet. Sci. Lett. 540, 116249. https://doi.org/10.1016/j.epsl.2020.116249.
Ernst, R.E., Youbi, N., 2017. How large Igneous Provinces affect global climate, sometimes cause mass extinctions, and represent natural markers in the geological record. Palaeogeogr. Palaeoclimatol. Palaeoecol. 478, 30–52. https://doi.org/10.1016/j.palaeo.2017.03.014.
Etiope, G., Sherwood Lollar, B., 2013. Abiotic methane on Earth. Rev. Geophys. 51, 276–299. https://doi.org/10.1002/rog.20011.
Etiope, G., Fridriksson, T., Italiano, F., Winiwarter, W., Theloke, J., 2007. Natural emissions of methane from geothermal and volcanic sources in Europe. J. Volcanol. Geotherm. Res. 165, 76–86. https://doi.org/10.1016/j.jvolgeores.2007.04.014.
Farrah, H., Pickering, W.F., 1978. Extraction of heavy metal ions sorbed on clays. Water Air Soil Pollut. 9, 491–498. https://doi.org/10.1007/BF00213544.
Fiebig, J., Woodland, A.B., Spangenberg, J.E., Oshmann, W., 2007. Natural evidence for rapid abiogenic hydrothermal generation of CH_4. Geochim. Cosmochim. Ac. 71, 3028–3039. https://doi.org/10.1016/j.gca.2007.04.010.
Fitzgerald, W.F., Lamborg, C.H., 2014. Geochemistry of mercury in the environment. Treatise Geochem. 11, 91–129. https://doi.org/10.1016/B978-0-08-095975-7.00904-9.
Fitzgerald, W.F., Lamborg, C.H., Hammerschmidt, C.R., 2007. Marine biogeochemical cycling of mercury. Chem. Rev. 107, 641–662. https://doi.org/10.1021/cr050353m.
Font, E., Adatte, T., Sial, A.N., de Lacerda, L.D., Keller, G., Punekar, J., 2016. Mercury anomaly, Deccan volcanism, and the end-Cretaceous mass extinction. Geology 44, 171–174. https://doi.org/10.1130/G37451.1.
Font, E., Adatte, T., Andrade, M., Keller, G., Bitchong, A.M., Carvallo, C., Ferreira, J., Diogo, Z., Mirão, J., 2018. Deccan volcanism induced high-stress environment during the Cretaceous-Paleogene transition at Zumaia, Spain: evidence from magnetic, mineralogical and biostratigraphic records. Earth Planet. Sci. Lett. 484, 53–66. https://doi.org/10.1016/j.epsl.2017.11.055.
Gehrke, G.E., Blum, J.D., Meyers, P.A., 2009. The geochemical behavior and isotopic composition of Hg in a mid-Pleistocene western Mediterranean sapropel. Geochim. Cosmochim. Ac. 73, 1651–1665. https://doi.org/10.1016/j.gca.2008.12.012.
Giggenbach, W.F., 1980. Geothermal gas equilibria. Geochim. Cosmochim. Ac. 44, 2021–2032. https://doi.org/10.1016/0016-7037(80)90200-8.
Gong, Q., Wang, X., Zhao, L., Grasby, S.E., Chen, Z.Q., Zhang, L., Li, Y., Cao, L., Li, Z., 2017. Mercury spikes suggest volcanic driver of the Ordovician-Silurian mass extinction. Sci. Rep. 7, 5304. https://doi.org/10.1038/s41598-017-05524-5.
Bond, D.P.G., Grasby, S.E., 2020. Late Ordovician mass extinction caused by volcanism, warming, and anoxia, not cooling and glaciation. Geology. https://doi.org/10.1130/G47377.1.
Grasby, S.E., Sanei, H., Beauchamp, B., Chen, Z.H., 2013. Mercury deposition through the Permo-Triassic biotic crisis. Chem. Geol. 351, 209–216. https://doi.org/10.1016/j.chemgeo.2013.05.022.
Grasby, S.E., Beauchamp, B., Bond, D.P.G., Wignall, P.B., Sanei, H., 2016. Mercury anomalies associated with three extinction events (Capitanian crisis, latest Permian extinction and the Smithian/Spathian extinction) in NW Pangea. Geol. Mag. 153, 285–297. https://doi.org/10.1017/S0016756815000436.
Grasby, S.E., Shen, W., Yin, R., Gleason, J.D., Blum, J.D., Lepak, R.F., Hurley, J.P., Beauchamp, B., 2017. Isotopic signatures of mercury contamination in latest Permian oceans. Geology 45, 55–58. https://doi.org/10.1130/G38487.1.
Grasby, S.E., Them, T.R., Chen, Z., Yin, R., Ardakani, O.H., 2019. Mercury as a proxy for volcanic emissions in the geologic record. Earth-Sci. Rev. 196, 102880. https://doi.org/10.1016/j.earscirev.2019.102880.
Grasby, S.E., Liu, X., Yin, R., Ernst, R.E., Chen, Z., 2020. Toxic mercury pulses into late Permian terrestrial and marine environments. Geology 48, 830–833. https://doi.org/10.1130/G47295.1.
Hallam, A., Wignall, P.B., 1997. Mass Extinctions and their Aftermath. Oxford University Press, Oxford.
Han, D.S., Orillano, M., Khodary, A., Duan, Y., Batchelor, B., Abdel-Wahab, A., 2014. Reactive iron sulfide (FeS)-supported ultrafiltration for removal of mercury (Hg(II)) from water. Water Res. 53, 310–321. https://doi.org/10.1016/j.watres.2014.01.033.
Henehan, M.J., Hull, P.M., Penman, D.E., Rae, J.W., Schmidt, D.N., 2016. Biogeochemical significance of pelagic ecosystem function: an end-Cretaceous case study. Philos. Trans. R. Soc. B 371, 20150510. https://doi.org/10.1098/rstb.2015.0510.
Holland, H.D., 1984. The Chemical Evolution of the Atmosphere and Oceans. Princeton University Press, Princeton, NJ.
Holmes, C.D., Jacob, D.J., Corbitt, E.S., Mao, J., Yang, X., Talbot, R., Slemr, F., 2010. Global atmospheric model for mercury including oxidation by bromine atoms. Atmos. Chem. Phys. 10, 12037–12057. https://doi.org/10.5194/acp-10-12037-2010.
House, M.R., 2002. Strength, timing, setting and cause of mid-Palaeozoic extinctions. Palaeogeogr. Palaeoclimatol. Palaeoecol. 181, 5–25. https://doi.org/10.1016/S0031-0182(01)00471-0.
Hull, P.M., Bornemann, A., Penman, D.E., Henehan, M.J., Norris, R.D., Wilson, P.A., Blum, P., Alegret, L., Batenburg, S.J., Bown, P.R., Bralower, T.J., 2020. On impact and volcanism across the Cretaceous-Paleogene boundary. Science 367, 266–272. https://doi.org/10.1126/science.aay5055.
Huybers, P., Denton, G., 2008. Antarctic temperature at orbital timescales controlled by local summer duration. Nat. Geosci. 1, 787–792. https://doi.org/10.1038/ngeo311.
Jay, A.E., Widdowson, M., 2008. Stratigraphy, structure and volcanology of the SE Deccan continental flood basalt province: Implications for eruptive extent and volumes. J. Geol. Soc. Lond. 165, 177–188. https://doi.org/10.1144/0016-76492006-062.
Jones, D.S., Martini, A.M., Fike, D.A., Kaiho, K., 2017. A volcanic trigger for the late Ordovician mass extinction? Mercury data from South China and Laurentia. Geology 45, 631–634. https://doi.org/10.1130/G38940.1.
Kale, V.S., Dole, G., Shandilya, P., Pande, K., 2020. Stratigraphy and correlations in Deccan Volcanic Province, India: Quo vadis? Geol. Soc. Am. Bull. 132, 588–607. https://doi.org/10.1130/B35018.1.
Keller, G., 1993. The Cretaceous-Tertiary boundary transition in the Antarctic Ocean and its global implications. Mar. Micropaleontol. 21, 1–45. https://doi.org/10.1016/0377-8398(93)90010-U.
Keller, G., 2003. Biotic effects of impacts and volcanism. Earth Planet. Sci. Lett. 215, 249–264. https://doi.org/10.1016/S0012-821X(03)00390-X.
Keller, G., 2004. Low-diversity, late Maastrichtian and early Danian planktic foraminiferal assemblages of the eastern Tethys. J. Foraminiferal Res. 34, 49–73. https://doi.org/10.2113/0340049.
Keller, G., 2014. Deccan volcanism, the Chicxulub impact, and the end-Cretaceous mass extinction: Coincidence? Cause and effect? In: Keller, G., Kerr, A.C. (Eds.), Volcanism, Impacts, and Mass Extinctions: Causes and Effects. Geol. Soc. Am, vol. 505. pp. 57–89. https://doi.org/10.1130/2014.2505(03).
Keller, G., Abramovich, S., 2009. Lilliput effect in late Maastrichtian planktic foraminifera: Response to environmental stress. Paleoclimatol. Paleoecol. Paleogeogr. 284, 47–62. https://doi.org/10.1016/j.palaeo.2009.08.029.
Keller, G., Benjamini, C., 1991. Paleoenvironment of the eastern Tethys in the early Paleocene. Palaios 6, 439–464. https://doi.org/10.2307/3514984.
Keller, G., Li, L., MacLeod, N., 1995. The Cretaceous/Tertiary boundary stratotype section at El Kef, Tunisia: how catastrophic was the mass extinction? Paleogeogr. Paleoclimat. Paleoecol. 119, 221–254. https://doi.org/10.1016/0031-0182(95)00009-7.
Keller, G., Adatte, T., Burns, S.J., Tantawy, A.A., 2002a. High-stress paleoenvironment during the late Maastrichtian to early Paleocene in Central Egypt. Paleogeogr. Paleoclimat. Paleoecol. 187, 35–60. https://doi.org/10.1016/S0031-0182(02)00504-7.
Keller, G., Adatte, T., Gardin, S., Bartolini, A., Bajpai, S., 2008. Main Deccan volcanism phase ends at K-T mass extinction: evidence from the Krishna-Godavari Basin, SE India. Earth Planet. Sci. Lett. 268, 293–311. https://doi.org/10.1016/j.epsl.2008.01.015.
Keller, G., Bhowmick, P.K., Upadhyay, H., Dave, A., Reddy, A.N., Jaiprakash, B.C., Adatte, T., 2011. Deccan volcanism linked to the Cretaceous-Tertiary boundary (KTB) mass extinction: New evidence from ONGC wells in the Krishna-Godavari Basin, India. J. Geol. Soc. India 78, 399–428. https://doi.org/10.1007/s12594-011-0107-3.
Keller, G., Adatte, T., Bhowmick, P.K., Upadhyay, H., Dave, A., Reddy, A.N., Jaiprakash, B.C., 2012. Nature and timing of extinctions in Cretaceous-Tertiary planktic foraminifera preserved in Deccan intertrappean sediments of the Krishna–Godavari Basin, India. Earth Planet. Sci. Lett. 341, 211–221. https://doi.org/10.1016/j.epsl.2012.06.021.
Keller, G., Khozyem, H., Adatte, T., Malarkodi, N., Spangenberg, J.E., Stinnesbeck, W., 2013. Chicxulub impact spherules in the North Atlantic and Caribbean: age constraints and Cretaceous–Tertiary boundary hiatus. Geol. Mag. 150, 885–907. https://doi.org/10.1017/S0016756812001069.
Keller, G., Punekar, J., Mateo, P., 2016. Upheavals during the late Maastrichtian: Volcanism, climate and faunal events preceding the end-Cretaceous mass extinction. Paleogeogr. Paleoclimat. Paleoecol. 441, 137–151. https://doi.org/10.1016/j.palaeo.2015.06.034.
Keller, G., Mateo, P., Punekar, J., Khozyem, H., Gertsch, B., Spangenberg, J., Bitchong, A.M., Adatte, T., 2018. Environmental changes during the Cretaceous-Paleogene mass extinction and Paleocene-Eocene thermal maximum: Implications for the Anthropocene. Gondwana Res. 56, 69–89. https://doi.org/10.1016/j.gr.2017.12.002.
Khadri, S., Subbarao, K., Hooper, P., Walsh, J., 1988. Stratigraphy of the Thakurvadi Formation, Western Deccan Basalt Province, India. Volcanol. Geol. Soc. India Mem. 10, 281–304.
Kim, C.S., Rytuba, J.J., Brown, G.E., 2004. EXAFS study of mercury(II) sorption to Fe- and Al-(hydr)oxides: I. Effects of pH. J. Colloid Interface Sci. 271, 1–15. https://doi.org/10.1016/s0021-9797(03)00330-8.
Kongchum, M., Hudnall, W.H., Delaune, R., 2011. Relationship between sediment clay minerals and total mercury. J. Environ. Sci. Health A 46, 534–539. https://doi.org/10.1080/10934529.2011.551745.
Krupp, R., 1988. Physicochemical aspects of mercury metallogenesis. Chem. Geol. 69, 345–356. https://doi.org/10.1016/0009-2541(88)90045-9.
Li, L., Keller, G., 1998a. Abrupt deep-sea warming at the end of the Cretaceous. Geology 26, 995–998. https://doi.org/10.1130/0091-7613(1998)026<0995:ADSWAT>2.3.CO;2.
Li, L., Keller, G., 1998b. Diversification and extinction in Campanian-Maastrichtian planktic foraminifera of northwestern Tunisia. Eclogae Geol. Helv. 91, 75–102.
Mangold, J.E., Park, C.M., Liljestrand, H.M., Katz, L.E., 2014. Surface complexation modeling of Hg(II) adsorption at the goethite/water interface using the charge distribution Multi-Site Complexation (CD-MUSIC) model. J. Colloid Interface Sci. 418, 147–161. https://doi.org/10.1016/j.jcis.2013.10.066.
Mateo, P., Keller, G., Adatte, T., Spangenberg, J.E., 2016. Mass wasting and hiatuses during the Cretaceous-Tertiary transition in the North Atlantic: Relationship to the Chicxulub impact? Paleogeogr. Paleoclimat. Paleoecol. 441, 96–115. https://doi.org/10.1016/j.palaeo.2015.01.019.
Mateo, P., Keller, G., Punekar, J., Spangenberg, E., 2017. Early to late Maastrichtian environmental changes in the Indian Ocean compared with Tethys and South Atlantic. Paleogeogr. Paleoclimatol. Paloecol. 478, 121–138. https://doi.org/10.1016/j.palaeo.2017.01.027.

Mclean, D.M., 1985. Mantle degassing induced dead ocean in the Cretaceous-Tertiary transition. In: Sundquist, E.T., Broecker, W.S. (Eds.), The Carbon Cycle and Atmospheric CO2: Natural Variations Archean to Present. Geophys. Monogr. Ser, vol. 32. pp. 493–503. https://doi.org/10.1029/GM032p0493.

Morford, J.L., Emerson, S., 1999. The geochemistry of redox sensitive trace metals in sediments. Geochim. Cosmochim. Ac. 63, 1735–1750. https://doi.org/10.1016/S0016-7037(99)00126-X.

Outridge, P.M., Sanei, H., Stern, G.A., Hamilton, P.B., Goodarzi, F., 2007. Evidence for control of mercury accumulation in sediments by variations of aquatic primary productivity in Canadian High Arctic lakes. Environ. Sci. Technol. 41, 5259–5265. https://doi.org/10.1021/es070408x.

Percival, L.M.E., Witt, M.L.I., Mather, T.A., Hermoso, M., Jenkyns, H.C., Hesselbo, S.P., Al-Suwaidi, A.H., Storm, M.S., Xu, W., Ruhl, M., 2015. Globally enhanced mercury deposition during the end-Pliensbachian extinction and Toarcian OAE: a link to the Karoo–Ferrar Large Igneous Province. Earth Planet. Sci. Lett. 428, 267–280. https://doi.org/10.1016/j.epsl.2015.06.064.

Percival, L.M., Ruhl, M., Hesselbo, S.P., Jenkyns, H.C., Mather, T.A., Whiteside, J.H., 2017. Mercury evidence for pulsed volcanism during the end-Triassic mass extinction. P. Natl. Acad. Sci. USA 114, 7929–7934. https://doi.org/10.1073/pnas.1705378114.

Percival, L.M.E., Jenkyns, H.C., Mather, T.A., Dickson, A.J., Batenburg, S.J., Ruhl, M., Hesselbo, S.P., Barclay, R., Jarvis, I., Robinson, S.A., Woelders, L., 2018. Does Large Igneous Province volcanism always perturb the mercury cycle? Comparing the records of Oceanic Anoxic event 2 and the end-Cretaceous to other Mesozoic events. Am. J. Sci. 318, 799–860. https://doi.org/10.2475/08.2018.01.

Pirrone, N., Cinnirella, S., Feng, X., Finkelman, R.B., Friedli, H.R., Leaner, J., Mason, R., Mukherjee, A.B., Stracher, G.B., Streets, D.G., Telmer, K., 2010. Global mercury emissions to the atmosphere from anthropogenic and natural sources. Atmos. Chem. Phys. Discuss. 10, 4719–4752. https://doi.org/10.5194/acp-10-5951-2010.

Punekar, J., Mateo, P., Keller, G., 2014a. Effects of Deccan volcanism on paleoenvironment and planktic foraminifera: A global survey. In: Keller, G., Kerr, A.C. (Eds.), Volcanism, Impacts, and Mass Extinctions: Causes and Effects. Geol. Soc. Am, vol. 505. pp. 91–116. https://doi.org/10.1130/2014.2505(04).

Punekar, J., Keller, G., Khozyem, H., Hamming, C., Adatte, T., Tantawy, A.A., Spangenberg, J.E., 2014b. Late Maastrichtian–early Danian high-stress environments and delayed recovery linked to Deccan volcanism. Cretac. Res. 49, 63–82. https://doi.org/10.1016/j.cretres.2014.01.002.

Punekar, J., Keller, G., Khozyem, H.M., Adatte, T., Font, E., Spangenberg, J., 2016. A multi-proxy approach to decode the end-Cretaceous mass extinction. Paleogeogr. Paleoclimatol. Paloecol. 441, 116–136. https://doi.org/10.1016/j.palaeo.2015.08.025.

Pyle, D.M., Mather, T.A., 2003. The importance of volcanic emissions for the global atmospheric mercury cycle. Atmos. Environ. 37, 5115–5124. https://doi.org/10.1016/j.atmosenv.2003.07.011.

Renne, P.R., Sprain, C.J., Richards, M.A., Self, S., Vanderkluysen, L., Pande, K., 2015. State shift in Deccan volcanism at the Cretaceous-Paleogene boundary, possibly induced by impact. Science 350, 76–78. https://doi.org/10.1126/science.aac7549.

Richards, M.A., Alvarez, W., Self, S., Karlstrom, L., Renne, P.R., Manga, M., Sprain, C.J., Smit, J., Vanderkluysen, L., Gibson, S.A., 2015. Triggering of the largest Deccan eruptions by the Chicxulub impact. Geol. Soc. Am. Bull. 127, 1507–1520. https://doi.org/10.1130/B31167.1.

Robock, A., 2000. Volcanic eruptions and climate. Rev. Geophys. 38, 191–219. https://doi.org/10.1029/1998RG000054.

Sanei, H., Grasby, S.E., Beauchamp, B., 2012. Latest Permian mercury anomalies. Geology 40, 63–66. https://doi.org/10.1130/G32596.1.

Schöbel, S., de Wall, H., Ganerød, M., Pandit, M.K., Rolf, C., 2014. Magnetostratigraphy and 40Ar–39Ar geochronology of the Malwa Plateau region (Northern Deccan Traps), central western India: significance and correlation with the main Deccan Large Igneous Province sequences. J. Asian Earth Sci. 89, 28–45. https://doi.org/10.1016/j.jseaes.2014.03.022.

Schoene, B., Samperton, K.M., Eddy, M.P., Keller, G., Adatte, T., Bowring, S.A., Khadri, S.F., Gertsch, B., 2015. U-Pb geochronology of the Deccan Traps and relation to the end-Cretaceous mass extinction. Science 347, 182–184. https://doi.org/10.1126/science.aaa0118.

Schoene, B., Eddy, M.P., Samperton, K.M., Keller, C.B., Keller, G., Adatte, T., Khadri, S.F., 2019. U-Pb constraints on pulsed eruption of the Deccan Traps across the end-Cretaceous mass extinction. Science 363, 862–866. https://doi.org/10.1126/science.aau2422.

Schoene, B., Eddy, M.P., Keller, C.B., Samperton, K.M., 2020. An evaluation of Deccan Traps eruption rates using geochronologic data. Geochronol. Discuss. https://doi.org/10.5194/gchron-2020-11. in review.

Schroeder, W.H., Munthe, J., 1998. Atmospheric mercury–an overview. Atmos. Environ. 32, 809–822. https://doi.org/10.1016/S1352-2310(97)00293-8.

Schulte, P., Alegret, L., Arenillas, I., Arz, J.A., Barton, P.J., Bown, P.R., Bralower, T.J., Christeson, G.L., Claeys, P., Cockell, C.S., Collins, G.S., Deutsch, A., Goldin, T.J., Goto, K., Grajales-Nishimura, J.M., Grieve, R.A.F., Gulick, S.P.S., Johnson, K.R., Kiessling, W., Koeberl, C., Kring, D.A., MacLeod, K.G., Matsui, T., Melosh, J., Montanari, A., Morgan, J.V., Neal, C.R., Nichols, D.J., Norris, R.D., Pierazzo, E., Ravizza, G., Rebolledo-Vieyra, M., Reimold, W.U., Robin, E., Salge, T., Speijer, R.P., Sweet, A.R., Urrutia-Fucugauchi, J., Vajda, V., Whalen, M.T., Willumsen, P.S., 2010. The Chicxulub asteroid impact and mass extinction at the Cretaceous-Paleogene boundary. Science 327, 1214–1218. https://doi.org/10.1126/science.1177265.

Scotese, C.R., 2013. Map Folio 16, KT Boundary (65.5 Ma, latest Maastrichtian). PALEOMAP PaleoAtlas for ArcGIS, volume 2, Cretaceous, PALEOMAP Project, Evanston, IL.

Self, S., Jay, A.E., Widdowson, M., Keszthelyi, L.P., 2008. Correlation of the Deccan and Rajahmundry Trap lavas: are these the longest and largest lava flows on Earth? J. Volcanol. Geotherm. Res. 172, 3–19. https://doi.org/10.1016/j.jvolgeores.2006.11.012.

Shen, J., Algeo, T.J., Chen, J., Planavsky, N.J., Feng, Q., Yu, J., Liu, J., 2019. Mercury in marine Ordovician/Silurian boundary sections of South China is sulfide-hosted and non-volcanic in origin. Earth Planet. Sci. Lett. 511, 130–140. https://doi.org/10.1016/j.epsl.2019.01.028.

Sheth, H., Pande, K., Vijayan, A., Sharma, K.K., Cucciniello, C., 2017. Recurrent early Cretaceous, Indo-Madagascar (89-86 Ma) and Deccan (66 Ma) alkaline magmatism in the Sarnu-Dandali complex, Rajasthan: 40Ar/39/Ar evidence and geodynamic significance. Lithos 284-285, 512–524. https://doi.org/10.1016/j.lithos.2017.05.005.

Sial, A.N., Chen, J., Lacerda, L.D., Frei, R., Tewari, V.C., Pandit, M.K., Gaucher, C., Ferreira, V.P., Cirilli, S., Peralta, S., Korte, C., 2016. Mercury enrichment and Hg isotopes in Cretaceous–Paleogene boundary successions: Links to volcanism and palaeoenvironmental impacts. Cretac. Res. 66, 60–81. https://doi.org/10.1016/j.cretres.2016.05.006.

Sial, A.N., Chen, J., Lacerda, L.D., Korte, C., Spangenberg, J.E., Silva-Tamayo, J.C., Gaucher, C., Ferreira, V.P., Barbosa, J.A., Pereira, N.S., Benigno, A.P., 2020. Globally enhanced Hg deposition and Hg isotopes in sections straddling the Permian–Triassic boundary: link to volcanism. Paleogeogr. Paleoclimatol. Paloecol. 540, 109537. https://doi.org/10.1016/j.palaeo.2019.109537.

Sprain, C.J., Renne, P.R., Vanderkluysen, L., Pande, K., Self, S., Mittal, T., 2019. The eruptive tempo of Deccan volcanism in relation to the Cretaceous-Paleogene boundary. Science 363, 866–870. https://doi.org/10.1126/science.aav1446.

Stern, G.A., Sanei, H., Roach, P., Delaronde, J., Outridge, P.M., 2009. Historical interrelated variations of mercury and aquatic organic matter in lake sediment cores from a subarctic lake in Yukon, Canada: further evidence toward the algal-mercury scavenging hypothesis. Environ. Sci. Technol. 43, 7684–7690. https://doi.org/10.1021/es902186s.

Stueben, D., Kramar, U., Berner, Z., Stinnesbeck, W., Keller, G., Adatte, T., 2002. Trace elements, stable isotopes, and clay mineralogy of the Elles II K–T boundary section in Tunisia: indications for sea level fluctuations and primary productivity. Paleogeogr. Paleoclimat. Paleoecol. 178, 321–345. https://doi.org/10.1016/S0031-0182(01)00401-1.

Stueben, D., Kramar, U., Berner, Z.A., Meudt, M., Keller, G., Abramovich, S., Adatte, T., Hambach, U., Stinnesbeck, W., 2003. Late Maastrichtian paleoclimatic and paleoceanographic changes inferred from Sr/Ca ratio and stable isotopes. Paleoclimatol. Paleoecol. Paleogeogr. 199, 107–127. https://doi.org/10.1016/S0031-0182(03)00499-1.

Taran, Y., Giggenbach, W., 2003. Geochemistry of light hydrocarbons in subduction-related volcanic and hydrothermal fluids. Soc. Econ. Geol. Sp. P. 10, 61–74.

Taylor, L.L., Banwart, S.A., Valdes, P.J., Leake, J.R., Beerling, D.J., 2012. Evaluating the effects of terrestrial ecosystems, climate and carbon dioxide on weathering over geologic time: a global-scale process-based approach. Philos. Trans. R. Soc. Lond. Ser. B Biol. Sci. 367, 565–582. https://doi.org/10.1098/rstb.2011.0251.

Them II, T.R., Jagoe, C.H., Caruthers, A.H., Gill, B.C., Grasby, S.E., Gröcke, D.R., Yin, R., Owens, J.D., 2019. Terrestrial sources as the primary delivery mechanism of mercury to the oceans across the Toarcian Oceanic Anoxic Event (Early Jurassic). Earth Planet. Sci. Lett. 507, 62–72. https://doi.org/10.1016/j.epsl.2018.11.029.

Thibault, N., Husson, D., 2016. Climatic fluctuations and sea-surface water circulation patterns at the end of the Cretaceous era: Calcareous nannofossil evidence. Palaeogeogr. Palaeoclimatol. Palaeoecol. 441, 152–164. https://doi.org/10.1016/j.palaeo.2015.07.049.

Thibault, N., Galbrun, B., Gardin, S., Minoletti, F., Le Callonnec, L., 2016. The end-Cretaceous in the southwestern Tethys (Elles, Tunisia): orbital calibration of paleoenvironmental events before the mass extinction. Int. J. Earth Sci. 105, 771–795. https://doi.org/10.1007/s00531-015-1192-0.

Thibodeau, A.M., Bergquist, B.A., 2017. Do mercury isotopes record the signature of massive volcanism in marine sedimentary records? Geology 45, 95–96. https://doi.org/10.1130/focus012017.1.

Thibodeau, A.M., Ritterbush, K., Yager, J.A., West, A.J., Ibarra, Y., Bottjer, D.J., Berelson, W.M., Bergquist, B.A., Corsetti, F.A., 2016. Mercury anomalies and the timing of biotic recovery following the end-Triassic mass extinction. Na. Commun. 7, 11147. https://doi.org/10.1038/ncomms11147.

Tribovillard, N., Algeo, T.J., Lyons, T., Riboulleau, A., 2006. Trace metals as paleoredox and paleoproductivity proxies: an update. Chem. Geol. 232, 12–32. https://doi.org/10.1016/j.chemgeo.2006.02.012.

Verma, O., Khosla, A., 2019. Developments in the stratigraphy of the Deccan Volcanic Province, peninsular India. Compt. Rendus Geosci. 351, 461–476. https://doi.org/10.1016/j.crte.2019.10.002.

Westerhold, T., Röhl, U., Raffi, I., Fornaciari, E., Monechi, S., Reale, V., Bowles, J., Evans, H.F., 2008. Astronomical calibration of the Paleocene time. Palaeogeogr. Palaeoclimatol. Palaeoecol. 257, 377–403. https://doi.org/10.1016/j.palaeo.2007.09.016.

Wolfenden, S., Charnock, J.M., Hilton, J., Livens, F.R., Vaughan, D.J., 2005. Sulfide species as a sink for mercury in lake sediments. Environ. Sci. Technol. 39, 6644–6648. https://doi.org/10.1021/es048874z.

Yang, Y., Liu, J., Liu, F., Wang, Z., Miao, S., 2018. Molecular-level insights into mercury removal mechanism by pyrite. J. Hazard. Mater. 344, 104–112. https://doi.org/10.1016/j.jhazmat.2017.10.011.